

ISTANBUL TECHNICAL UNIVERSITY ★ GRADUATE SCHOOL OF SCIENCE
ENGINEERING AND TECHNOLOGY

**PROBING THE ARRANGEMENT OF THE CONFORMATIONAL
ENSEMBLES OF DNAK**



M.Sc. THESIS

Melis KORKMAZ

Department of Molecular Biology-Genetics and Biotechnology

Molecular Biology, Genetics and Biotechnology Programme

Thesis Advisor: Assoc. Prof. Dr. Gizem DİNLER DOĞANAY

NOVEMBER 2018

ISTANBUL TECHNICAL UNIVERSITY ★ GRADUATE SCHOOL OF SCIENCE
ENGINEERING AND TECHNOLOGY

**PROBING THE ARRANGEMENT OF THE CONFORMATIONAL
ENSEMBLES OF DNAK**



M.Sc. THESIS

Melis KORKMAZ

(521151132)

Department of Molecular Biology-Genetics and Biotechnology

Molecular Biology, Genetics and Biotechnology Programme

Thesis Advisor: Assoc. Prof. Dr. Gizem DİNLER DOĞANAY

NOVEMBER 2018

ISTANBUL TEKNİK ÜNİVERSİTESİ ★ FEN BİLİMLERİ ENSTİTÜSÜ

**DNAK NÜKLEOTİT BAĞLANMA DOMENİNİN OLUŞTURDUĞU
KONFORMASYONAL POPÜLASYONLARIN ARAŞTIRILMASI**

YÜKSEK LİSANS TEZİ

Melis KORKMAZ

(521151132)

Moleküler Biyoloji Genetik ve Biyoteknoloji Anabilim Dalı

Moleküler Biyoloji Genetik ve Biyoteknoloji Programı

Tez Danışmanı: Doç. Dr. Gizem DİNLER DOĞANAY

KASIM 2018

Melis KORKMAZ, a M.Sc. student of ITU **Graduate School of Science, Engineering and Technology** student ID **521151132**, successfully defended the thesis entitled “**PROBING THE ARRANGEMENT OF THE CONFORMATIONAL ENSEMBLES OF DNAK**”, which she prepared after fulfilling the requirements specified in the associated legislations, before the jury whose signatures are below.

Thesis Advisor: **Assoc. Prof. Gizem DİNLER DOĞANAY**

Istanbul Technical University

Jury Members: **Asst. Prof. Bülent BALTA**

Istanbul Technical University

Asst. Prof. Bahar Soğutmaz ÖZDEMİR

Yeditepe University

Date of Submission : 12 November 2018

Date of Defense : 15 November 2018





To my lovely family and my love,



FOREWORD

First of all, I would like to express my sincere gratitude to my supervisor Assoc. Prof. Dr. Gizem DİNLER DOĞANAY for her constant encouragement, guidance and patience throughout my M.Sc. education.

I would like to thank TUBITAK (The Scientific and Technical Research Council of Turkey) to support financially for the 1007 project whose number is 115G078.

I owe a debt gratitude to my special colleague friend Özge TATLI. She always supported and shared all her knowledge with me.

I would also like to express my special thanks to Baran Dingilođlu for academical help to perform IMS analysis.

I also thank to the colleagues in our research group for their motivation both in the school and in my daily life. This lab was a place where I learned not only business awareness but also being indulgent on academic motivation.

I must present my deepest thanks to my family and my beloved friends for their unlimited love, endless support and patience through my whole life.

November 2018

Melis KORKMAZ



ABBREVIATIONS

ADP	: Adenosine diphosphate
Amp	: Ampicillin
APS	: Ammonium persulfate
ATP	: Adenosine triphosphate
ATPase	: Adenosine triphosphatase
CD	: Circular dichroism
DEAE	: Diethylaminoethyl
DNA	: Deoxyribonucleic acid
ddH₂O	: Distilled water
ddH₂O	: Double distilled water
DnaJ	: <i>Escherichia coli</i> homolog of Hsp40
DnaK	: <i>Escherichia coli</i> homolog of Hsp70
DTT	: Dithiothreitol
<i>E. coli</i>	: <i>Escherichia coli</i>
EDTA	: Ethylenediaminetetraacetic acid
ER	: Endoplasmic reticulum
FPLC	: Fast protein liquid chromatography
GrpE	: Nucleotide exchange factor homolog in <i>E. coli</i>
H₂O	: Water
HCl	: Hydrochloric acid
HEPES	: 4-(2-hydroxyethyl)-1-piperazineethanesulfonic acid
hHsp70	: Human homolog of Hsp70
Hsc70	: Constitutively expressed Hsp70 homolog
Hsp	: Heat Shock Protein
IMS	: Ion-mobility mass spectrometry
IPTG	: Isopropyl β-D-1-thiogalactopyranoside
KCl	: Potassium chloride
MgCl₂	: Magnesium chloride
Mg(OAc)₂	: Magnesium acetate
NADH	: Nicotinamide adenine dinucleotide hydrate
NaOH	: Sodium hydroxide
NBD	: Nucleotide binding domain
NMR	: Nuclear magnetic resonance
OD	: Optical density
PDB	: Protein Data Bank
PEP	: Phosphoenolpyruvic acid
P_i	: Inorganic phosphate
PK	: Pyruvate Kinase
PMSF	: Phenylmethanesulfonyl fluoride
SBD	: Substrate binding domain
SDS-PAGE	: Sodium dodecyl sulfate polyacrylamide gel electrophoresis
TEMED	: Tetramethylethylenediamine
UV	: Ultraviolet



TABLE OF CONTENTS

	<u>Page</u>
TABLE OF CONTENTS	xiii
LIST OF TABLES	xv
LIST OF FIGURES	xvii
SUMMARY	xix
ÖZET	xxi
1. INTRODUCTION	1
1.1 Heat Shock Proteins	1
1.2 Heat Shock Proteins Family	2
1.3 Heat Shock Protein 70 (Hsp70).....	3
1.4 Functions of Hsp70	4
1.5 Molecular Mechanism of Hsp70	5
1.6 Structure of Hsp70.....	7
1.7 Dynamic Studies of Hsp70.....	8
1.7.1 Secondary structure analysis using circular dichroism.....	9
1.7.2 Ion-mobility spectrometry	10
1.8 Aim of This Study	11
2. MATERIALS AND METHODS	13
2.1 Materials	13
2.1.1 Laboratory equipments	13
2.1.2 Chemicals and enzymes	13
2.1.3 Commercial kits	13
2.1.4 Bacterial strains.....	13
2.1.5 Buffer and solutions.....	13
2.2 Methods	13
2.2.1 Preperation of DH5 α competent cells.....	13
2.2.2 Plasmid transformation of competent cells.....	14
2.2.3 Plasmid DNA preparation.....	14
2.2.4 Preparation of BB1553 competent cells	15
2.2.5 Plasmid transformation of BB1553 competent cells	15
2.2.6 Growth of the transformed BB1553 cells	16
2.2.7 Preparation of cell extract	16
2.2.8 Control of induction.....	16
2.2.9 DnaK purification with DEAE Sepharose FF column.....	16
2.2.10 DnaK purification with ATP-agarose column	17
2.2.11 Column regeneration.....	18
2.2.12 ATPase measurement	18
2.2.13 Circular dichroism (CD) measurements	19
2.2.14 Ion-mobility spectrometry	19

3. RESULTS	21
3.1 Analysis of Sequenced Data of Wild-type DnaK ₃₉₂ and DnaK ₃₈₈ in <i>E. coli</i>	21
3.2 Expression of the Wild-type DnaK ₃₉₂ and DnaK ₃₈₈ in <i>E. coli</i>	21
3.3. Purification of the Wild-type DnaK ₃₉₂ and DnaK ₃₈₈ in <i>E. coli</i>	22
3.4 Result of Enzyme-coupled ATPase Assay	25
3.5 Secondary Structure Analysis of DnaK ₃₉₂ and DnaK ₃₈₈	26
3.6 Conformational analysis of DnaK ₃₉₂ and DnaK ₃₈₈ via Ion-Mobility Spectrometry.....	27
4. DISCUSSION.....	33
REFERENCES	35
APPENDICES	39
CURRICULUM VITAE.....	55



LIST OF TABLES

	<u>Page</u>
Table 1.1: Major heat shock protein families, their approximate molecular weight, prokaryotic family members, eukaryotic localizations, and functions.....	3
Table A.1: Laboratory equipments used in the experiments.....	41
Table B.1: Chemicals and Enzymes used in the experiments.....	43





LIST OF FIGURES

	<u>Page</u>
Figure 1.1: Models for heat shock proteins, folding the newly-synthesized protein in cytosol for Eubacteria, Archaea and Eukarya (Adapted from Hartl and Hayer-Hartl, 2002).....	1
Figure 1.2: Crystal Structure of DnaK (Hsp70 homolog) in the ADP-bound closed conformation (left, PDB ID 2KHO) and in the ATP-bound open conformation (right, 4B9Q15) (Adapted from Kityk <i>et al.</i> , 2015).....	5
Figure 1.3: Hsp70 machinery. (Adapted from Brehme and Voisine, 2016). ATP is shown as dark grey, ADP is shown as light grey, substrate is shown as blue line, NBD is shown as light orange, SBD and lid are shown as orange, Hsp40 is shown as light blue, and Nucleotide exchange factor (NEF) is shown as red.....	6
Figure 1.4: Secondary structure representation of α -helix, β -sheet and random coil polypeptide chain (Taken from Wei, et al. 2014).	10
Figure 2.1: NADH-coupled ATPase assay.	18
Figure 3.1: Induction control of wild type DnaK ₃₉₂ and DnaK ₃₈₈ by SDS-PAGE results.	21
Figure 3.2: Anion Exchange Chromatogram of DnaK ₃₉₂ (above) and Anion exchange chromatography fractions of DnaK ₃₉₂ by SDS-PAGE (below).....	22
Figure 3.3: Anion Exchange Chromatogram of DnaK ₃₈₈ (above) and Anion exchange chromatography fractions of DnaK ₃₈₈ by SDS-PAGE (below).....	23
Figure 3.4: ATP Affinity Purification Chromatogram of DnaK ₃₉₂ (above), DnaK ₃₉₂ SDS-PAGE results from ATP affinity chromatography (below).	24
Figure 3.5: ATP Affinity Purification Chromatogram of DnaK ₃₈₈ (above), DnaK ₃₈₈ SDS-PAGE results from ATP affinity chromatography (below).	25
Figure 3.6: pH-dependent ATPase activity profiles of DnaK ₃₉₂ . Error bars on line represent standard deviation from 3 experiments.	26
Figure 3.7: pH-dependent ATPase activity profiles of DnaK ₃₈₈ . Error bars on line represent standard deviation from 3 experiments.	26
Figure 3.8: Circular Dichroism spectra results of DnaK ₃₉₂ and DnaK ₃₈₈	27
Figure 3.9: Charge state distributions of purified DnaK ₃₉₂ protein in a range of pH values.	28
Figure 3.10: IMS analysis of purified DnaK ₃₉₂ protein in a range of pH values. The three-dimensional IMS spectra of DnaK ₃₉₂ is on the left, and the drift time distribution is on the right.	29
Figure 3.11: Charge state distributions of purified DnaK ₃₈₈ protein in a range of pH values	30
Figure 3.12: IMS analysis of purified DnaK ₃₈₈ protein in a range of pH values. The three-dimensional IMS spectra of DnaK ₃₈₈ is on the left, and the drift time distribution is on the right.	31



PROBING THE ARRANGEMENT OF THE CONFORMATIONAL ENSEMBLES OF DnaK

SUMMARY

Proteins are macromolecules that are important for life. Proteins have various cellular functions, which rely on their correctly folded three-dimensional (3-D) structure. Proper folding of nascent protein chains that require assistance to get their native state is accomplished by Heat shock proteins (Hsps) also called as “molecular chaperons”. Hsps are highly conserved family of proteins from bacteria to human. They are not only expressed in normal conditions, but also are expressed in different stress conditions. They participate in numerous cellular functions, which include preventing aggregation, assisting protein folding, refolding of denatured proteins, and degradation. Hsp70s can recognize unfolded, misfolded and aggregated forms of the proteins from their exposed hydrophobic groove. There is a cycle of HSP70s sustained by the use of ATP. During this cycle client polypeptides are get folded by HSP70s successfully to their native states. Hsp70 proteins have two main domains, which are a highly conserved 44 kDa, N-terminal nucleotide binding domain (NBD) and a variable 25 kDa, C-terminal substrate binding domain (SBD). NBD comprises two main lobes and these lobes are divided into upper-lower part and right-left part. SBD consist of two parts which are α -helical lid and β -sandwich subdomain. The α -helical lid covers over the polypeptide bound state. The β -sandwich binds to substrates with a hydrophobic groove. NBD and SBD are connected to each other with a highly conserved hydrophobic linker (GDVKDVLLL). Hydrophobic linker has a critical role in allosteric mechanism of Hsp70. Two different constructs of DnaK namely, DnaK₃₈₈ and DnaK₃₉₂, are used to investigate the interdomain communication mechanism by Swain *et al.* (2007). Both residues do not contain SBD. DnaK₃₉₂ contains a conserved hydrophobic ³⁸⁹VLLL³⁹² sequence of the interdomain linker, while DnaK₃₈₈ lacks this linker sequence. These investigations were shown with truncated DnaK constructs as presence or absence of linker. In the same study, the partial interdomain ³⁸⁹VLLL³⁹² linker sequence is found as active and critical for the communication of the ATPase domain and the SBD. It is shown that the construct DnaK₃₉₂ mimics very similar ATPase activity at the peptide bound state. It was reported that DnaK₃₉₂ has an ATPase activity that is similar to that of the substrate-stimulated form of DnaK. On the contrary, DnaK₃₈₈ has an ATPase activity that is similar to that of the unstimulated state of DnaK. In this study, we would like to detect the different adaptable conformations of the ATPase domain derived from the crucial ³⁸⁹VLLL³⁹² linker in equilibrium. We studied with an NBD variant which has a partial interdomain linker sequence ³⁸⁸VLLL³⁹² and with the NBD itself to investigate the arrangement of the conformational ensembles of Hsp70. These proteins are shown to be already folded after purification and they are found in APA state. It is shown by the native mass spectrometry charge state distribution. Our findings revealed that DnaK₃₉₂ has a charge shift behaviour observed at +14 charge state rather than the most effective charge of +13 charge state after pH 7.5 by native mass spectrometry. Below pH 7.5 there is

predominantly one population being observed; and with the pH increase, two distinct conformations of DnaK₃₉₂ were determined by ion-mobility mass spectrometry. pH alterations cause subtle conformational variations for DnaK₃₈₈, on the other hand, our complementary approach has shown the existence of a discrete allosterically active state of DnaK in the presence of partial linker using ion-mobility mass spectrometry.



DNAK NÜKLEOTİT BAĞLANMA DOMENİNİN OLUŞTURDUĞU KONFORMASYONAL POPÜLASYONLARIN ARAŞTIRILMASI

ÖZET

Proteinler, canlıların yaşamı açısından önemli olan makromoleküllerdendir. Proteinler çeşitli görevlere sahiptirler ve bu görevleri yerine getirebilmeleri için doğru 3-boyutlu konformasyonu kazanmaları gerekmektedir. Küçük proteinlerin bazıları başka bir proteine ihtiyaç duymadan katlanabilirken, uzun zincirli proteinler ribozomun dar yapısından dolayı ribozomun içinde katlanamazlar ve katlanabilmek için moleküler şaperon olarak adlandırılan ısı şok proteinlerine ihtiyaç duyarlar. Hatalı katlanan proteinler, diğer proteinlerin katlanmasını geciktirir ya da engellerler. DNA kontrolünde sentezlenen proteinlerin üçüncül yapılarını kazanmasını sağlamak ısı şok proteinlerinin görevidir. Hem hücre içinde hem de hücre dışında bulunabilen ısı şok proteinleri (Hsp) hücre membranlarında da gözlemlenirler. Isı şok proteinlerinin sentezi sadece normal koşullarda gerçekleşmez, aynı zamanda yüksek sıcaklık, pH değişimi, ağır metal, oksidatif ve kimyasal stres koşullarında sentezlenmeleri hızlanır. Isı şok protein çalışmaları 1960 yılının başlarında Ferruccio Ritossa'nın öncülüğünde, meyve sineği *Drosophila melanogaster* ile başlamıştır.

Isı şok proteinleri (moleküler şaperon) ailesinden olan 70 kDa ısı şok proteinleri (Hsp70s), evrimsel açıdan yüksek derecede korunmuş proteinlerdir. Hsp70'in, bakteriden ökaryotlara kadar bütün canlı organizmalarda önemli rolleri bulunmaktadır. Yeni sentezlenen proteinlerin katlanması, proteinlerin kümeleşmesinin engellenmesi, denatürasyondan korunması, yanlış katlanmış proteinlerin yeniden katlanması, proteinlerin translokasyonlarının sağlanması, hasara uğramış proteinlerin yıkılması Hsp70 tarafından gerçekleştirilir. Katlanmamış proteinlerin hidrofobik bölgeleri açığa çıkar ve Hsp70, katlanmamış proteinlerin hidrofobik bölgelerine hidrofobik etkileşim ile bağlanarak yanlış katlanmayı engeller. Bu sayede hidrofobik etkileşimden kaynaklanan kümeleşmeler engellenmiş olur. Hsp70 hücre içerisinde edindiği görevler dışında hücre homeostazisinde de görev alır. Tüm bu görevlere bakıldığında Hsp70'in hücrenin bekçisi gibi görev aldığını görüyoruz.

Proteinlerin yanlış katlanması, kümeleşmesi ya da çökmesi Alzheimer, Huntington, Parkinson, Kennedy gibi bazı nörodejeneratif hastalıklara sebep olabilir. Amiloid yapısındaki proteinler sinir sisteminde birikmeye başladıkları zaman nörodejeneratif hastalıklara sebep olduğu görülmüştür ve beta amyloid birikimini Hsp70 aktivitesinin engellediği keşfedilmiştir (Dou ve ark., 2003; Labrador-garrido ve ark., 2010). Parkinson hastalığına sebep olan α -sinüklein proteininin kümeleşmesinde Hsp70'in koruyucu olarak rol aldığı görülmüştür (Labrador-garrido ve ark., 2010). Alzheimer hastalarında yanlış katlanan tau proteinlerinin çözünürlüğü Hsp70 tarafından artırıldığı görülmüştür (Dou ve ark., 2003). Aynı zamanda Hsp70'in apoptoz yolağında anti-apoptotik protein olarak görev alır.

Çalışmamızda *Escherichia coli* Hsp70 homologu DnaK kullanıldı. DnaK amino (N) ucunda nükleotit bağlanma bölgesi (NBD) ve karboksil (C) ucunda substrat bağlanma

bölgesi (SBD) olmak üzere iki temel bölgeden oluşur. Bu iki temel bölgeyi birbirine bağlayan evrensel olarak oldukça korunmuş hidrofobik bir bağlaç bulunur. N ucunda bulunan 44 kDa'lık NBD ATPaz aktivitesi gösterirken, C ucunda bulunan 25 kDa'lık SBD substrat bağlar. Kristalografik yapılarına bakıldığı zaman NBD'nin iki ana lobdan oluştuğu ve bu lobların ise iki alt bölgeye, toplamda IA, IIA, IB, IIB olmak üzere 4 alt domene ayrıldığı görülür. SBD'in kristalografik yapısı incelendiğinde α -heliks ve β -tabaka olmak üzere iki kısım görülür. β -tabakasında substrat bağlama yarığı bulunurken, α -heliks kapak görevi görür ve substrat yarığa gelip tutunduğu zaman SBD'in üzerine kapanır.

NBD ve SBD arasında hidrofobik bağlacın sağladığı allosterik bir etkileşim vardır. ADP-bağlı durumda bu iki bölge birbirinden bağımsız davranırken, ATP-bağlı durumda birbirleriyle iletişime geçerek sıkı bir şekilde birbirlerine bağlanırlar. ATP-bağlı durumda NBD dengeli hale gelir, substrat bağlanma afinitesi düşer ve bu sırada SBD'in α -heliks kapak yapısı açıktır. ATP hidrolizlenip P_i ve ADP'ye dönüştüğünde substrat bağlanma afinitesinde artış gözlenir. ADP-bağlı durumda SBD'in α -heliks kapak yapısı SBD üzerine kapanır. Bu döngüye yardım eden iki çeşit ko-şaperon bulunur; ATP hidrolizini hızlandıran Hsp40 (DnaJ) ve oluşan nükleotitin değişimini sağlayan, Hsp70'i yeni döngüye hazırlayan nükleotit değişim faktörlerinden olan GrpE'dir. Gerçekleşen allosterik etkileşimde anahtar olarak rol alan bağlaç bölgesi bulunmaktadır. Bu bağlaç bölgesinin yapısı ve görevi tam olarak aydınlatılmadığı için SBD ve NBD arasındaki sinyal iletimi bilinmemektedir.

DnaK₃₉₂ proteininin NMR analizleri yapıldığında yapısında bulunun (³⁸⁸VLLL³⁹²) dizisinin NBD bölgesinin IA ve IIA lobları arasındaki yarığa bağlandığı gözlemlenmiştir (Zhuravleva and Gierasch, 2011). NMR sonuçlarında DnaK₃₉₂ proteininin yapısının substrat ile indüklenmiş yabanıl tip DnaK'nin yapısına benzediği ortaya çıkmıştır. Bu sebepten dolayı araştırmalarda yabanıl tip DnaK kullanmak yerine DnaK₃₉₂ proteininin kullanılması tercih edilmiştir.

Swain ve arkadaşları tarafından 2007 yılında gerçekleştirilen çalışmalarda, NBD bölgesi ve 9 amino asit içeren bağlayıcı bölgenin tamamını (³⁸³GDVKDVLLL³⁹²) içeren, SBD içermeyen DnaK₃₉₂ proteini kullanılmıştır. DnaK₃₉₂, bağlaç bölgesinde içerdiği (³⁸⁸VLLL³⁹²) dizisi sayesinde substrat tarafından uyarılmış yabanıl tip DnaK'yi taklit ettiği ve benzer pH-bağımlı profil oluşturduğu görülmüştür. DnaK₃₉₂ proteininin aksine bağlaç bölgesinde (³⁸⁸VLLL³⁹²) dizisini içermeyen DnaK₃₈₈ proteininin sonuçlarını bakıldığında, ATPaz aktivitesinin peptit bağlı olmayan yabanıl tip DnaK gibi davrandığı ve pH-bağımlı profillerinin benzer olduğu görülmüştür. DnaK₃₉₂ ve DnaK₃₈₈ proteinlerinin incelenmesiyle (³⁸⁸VLLL³⁹²) dizisinin SBD ve NBD bölgeleri arasındaki sinyal iletim mekanizmasını nasıl etkilediği gözlemlenmiştir. Çalışmanın sonucuna bakıldığında hidrofobik bağlaç bölgesinin (³⁸⁸VLLL³⁹²) dizisini içermesi allosterik etkileşimi sağlamakta, dizinin varlığında ve yokluğunda görevlerin farklı olduğu anlaşılmaktadır.

Bu çalışmada, daha önceki çalışmalarda olduğu gibi yabanıl tip DnaK₃₉₂ ve DnaK₃₈₈ plazmiti *DnaK* geni içermeyen *Escherichia coli* BB1553 kompetan hücrelerine transformasyon ile aktarılıp IPTG ile indükledi. Art arda gerçekleştirilen anyon değişim kromatografisi ve afinite kromatografisi ile proteinlerin saf hali elde edildi. DnaK proteininin ATP'ye bağlanma özelliği olduğu için afinite kromatografisi adımı bu özellik kullanılarak ATP-agaroz kolonu kullanıldı.

Dairesel dikroizm (CD) ışığı, hem sağ hem sol dairesel polarize ışığa dönüştürülür ve proteinin peptit bağlarının ışığı emmesiyle eliptiktik değeri bulunur. CD spektroskopisi

kullanılarak DnaK₃₉₂ ve DnaK₃₈₈ proteinlerinin ikincil yapısı ve kararlılığının önceki çalışmalar ile benzerlik gösterdiği görüldü.

DnaK₃₉₂ ve DnaK₃₈₈ için ATPaz aktivite ölçümleri yapılarak literatürde gösterilmiş olan pH'a bağımlı ATPaz aktivitesine etkilerinin olup olmadığı kanıtlanmaya çalışılmıştır. DnaK₃₉₂'nin, substratla uyarılan DnaK formuna benzer bir ATPaz aktivitesine sahip olduğu bildirilmiştir. Aksine, DnaK₃₈₈, uyarılmamış DnaK durumu ile benzer bir ATPase aktivitesine sahiptir. Bu çalışmada, denge durumunda (³⁸⁸VLLL³⁹²) dizisinin ATPaz bölgesinin farklı uyarlanabilir uyumlarını tespit etmek istiyoruz. Bu sonuca ulaşmak için doğal kütle spektrometresi ve iyon-hareketlilik kütle spektrometrisi yöntemleri kullanılmıştır.

İyon-hareketlilik kütle spektrometresi (IM-MS), iyonları elektrik alanı etkisi altında kütle/yük oranlarına göre ayıran analitik tekniktir. IM-MS'de elektrik alanı iyonları hızlandırırken, taşıyıcı tampon gazı ile iyonların çarpışması hızlarını yavaşlatır. İyonların dedektöre ulaşma süreleri biyomoleküllerin büyüklükleriyle orantılı olduğu için, biyomoleküller ne kadar büyük olursa dedektöre ulaşma süreleri de o kadar fazla olur.

Deneysel bulgularda, DnaK₃₉₂'nin doğal kütle spektrometresi ile yük dağılımına bakıldığında pH değerinin 7.5'in altındayken DnaK₃₉₂'nin en etkin yükü olan +13'ün yük durumu kayması sonucu +14 olduğu gözlemlenmiştir. DnaK₃₉₂'nin aksine, pH değerinin bazikliği arttıkça DnaK₃₈₈ en etkin olduğu yükünü korumuş kimyasal kayma gözlemlenmemiştir. DnaK₃₉₂ ile farklı pH denemeleriyle yapılan IM-MS çalışmalarında, pH 7.5'in altındayken ağırlıklı olarak tek popülasyon gözlemlenmiş, pH 7.5'in üzerindeyken belirgin iki farklı konformasyon belirlenmiştir. DnaK₃₈₈ için pH 6.5 ve 8.5 aralığında büyük konformasyonel değişikliklere neden olmadığı gözlemlenmiştir. Bu sonuçlar ışığında, bağlaç bölgesinde, (³⁸⁸VLLL³⁹²) dizisini içeren popülasyonun allosterik olarak aktif DnaK olduğu IM-MS ile gösterilmiştir.



1. INTRODUCTION

1.1 Heat Shock Proteins

Heat Shock Proteins (Hsps), which are also referred to as “molecular chaperones”, were initially studied by Ferruccio Ritossa's pioneering work on fruit fly *Drosophila melanogaster* at the beginning of the 1960s (Ritossa, 1962). Hsps were later found in all organisms such as eubacteria, archaea and eukarya (Figure 1.1). Hsp expressions are demonstrated to be induced upon exposure to different stress types such as heat shock, heavy metals, hypoxia, oxidative and toxic stress, infections in many cellular organisms. However, in 1980s, it has been understood that these Hsps are ubiquitously expressed in the cell even in the absence of stress (Craig *et al.*, 1982). Hsps are proteins, which are highly conserved family of proteins through evolution from bacteria to human. Numerous polypeptides need the assistance of molecular chaperons to acquire their final conformations. Under heat stress conditions, Hsps are expressed more to prevent denaturation and aggregation of proteins.

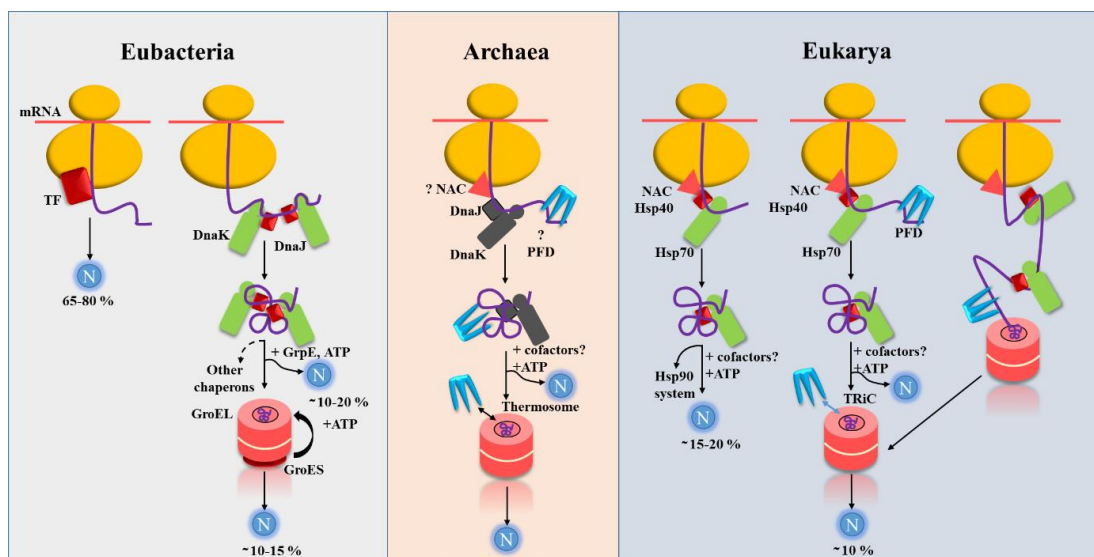


Figure 1.1: Models for heat shock proteins, folding the newly-synthesized protein in cytosol for Eubacteria, Archaea and Eukarya (Adapted from Hartl and Hayer-Hartl, 2002).

Their activities not only include playing a critical role in preventing harmful aggregation but also these proteins assist protein folding, refolding of denatured

proteins, degradation or oligomeric assembly, ubiquitination of irreversibly unfolded proteins and cellular transport, which have primary importance in cellular activities (Hendrick and Hartl, 1993; Hipp *et al.*, 2014).

1.2 Heat Shock Proteins Family

Heat shock proteins are named regarding to their molecular weights and they are classified into different families, such as, Hsp60, Hsp70 and Hsp90, which correspond to the members of heat shock proteins 60, 70 and 90 kilo Daltons, respectively (Ratheesh Kumar *et al.*, 2012). Hsps bind to non-native proteins and they prevent aggregation. Members of the heat shock proteins function as a network to perform variety of cell processes.

Many heat shock proteins interact with nucleotide exchange factors or other co-chaperone complexes such as GrpE and Hsp70-Hsp40 complex which is the core of a chaperone machinery (bacterial DnaK/DnaJ) or Hsp60-Hsp10 complex (bacterial GroEL/GroES), respectively. Hsp40 assists folding, transport and prevention of degradation of the substrate protein and regulates the ATP-dependent polypeptide-binding by Hsp70s (Fan *et al.*, 2003). These co-chaperones are fundamental activator of Hsp70 proteins and they also stimulate ATPase activity in nucleotide binding domain of Hsp70 (Alderson *et al.*, 2016). Hsp40 is involved in the recruitment of Hsp70s for distinct purposes including proteasomal degradation, import into mitochondria, conformational transition during signalling events, and disassembly of protein complexes (Young *et al.*, 2003). Hsp40s ensure the ATPase-stimulatory function with nucleotide exchange factor (NEF). The studies of NMR have proved that the ATPase domain is a part for DnaJ binding to DnaK (Bascos *et al.*, 2017). Hsp70s not only collaborate with Hsp40s but also interact with Hsp90, which is an ATP-dependent chaperone and associates with Hsp70s for protein folding, trafficking and turnover (Makhnevych and Houry, 2012; Pratt *et al.*, 2010). Major heat shock protein families are shown in Table 1.1, along with their eukaryotic localizations and their prokaryotic homologs.

Table 1.1: Major heat shock protein families, their approximate molecular weight, prokaryotic family members, eukaryotic localizations, and functions.

Protein family	Approximate Molecular Weight (kDa)	Prokaryotic family members	Eukaryotic localization	Function
sHsp	-	IbpA,IbpB	Cytosol / cell surface	Preventing the aggregation of heat denaturated proteins
Hsp60	60	GroEL (co-chaperone: GroES)	Mitochondria / chloroplast	Related with protein folding after its post-translational import to the mitochondria / chloroplast.
Hsp70	70	DnaK(co-chaperones: DnaJ,GrpE)	Cytosol/ nucleus/ER/ mitochondria/ chloroplast	Protein folding and unfolding, provides thermotolerance to the cell when exposed to heat stress. It also prevents protein folding into the mitochondria / chloroplast during post-translational import.
Hsp90	90	HtpG	Cytosol	Maintenance of cellular homeostasis.
Hsp100	100	ClpB, ClpA, ClpX	Cytosol	Rescue aggregated proteins and provide tolerance of extreme temperature to cells.

1.3 Heat Shock Protein 70 (Hsp70)

The stress-inducible Hsp70 molecular chaperons are the most ubiquitously expressed family members, which were identified for the first time in bacteria and shown to be upregulated in response to cellular stresses. Hsp70s are highly conserved protein along all species and expressed in various organisms from primitive organisms to complex multicellular organisms like human, namely DnaK in bacteria, Hsc70 in bovine and Hsp70 in human (Feder and Hofmann, 1999; Liang and MacRae, 1997). Hsp70 proteins of *Drosophila* have an amino acid identity in about 70% of their yeast and *E.coli* homologs. They are allosteric proteins and implement a number of chaperone functions in the cell both under stress and normal physiological conditions (Lai *et al.*, 2017). It is believed that Hsp70s bind to the hydrophobic regions that are revealed on the surface of denaturated polypeptides and prevent aggregation due to incorrect hydrophobic interactions (Uchida and Kanemori, 2018). Hsp70s reside in the cytosol of bacteria. In eukaryotes, Hsp70s are localized in membrane-bound organelles such

as nucleus, mitochondria, chloroplasts and endoplasmic reticulum or in cytosol to provide folding of immature polypeptides to their native conformation (Alderson *et al.*, 2016; Hartl and Hayer-Hartl, 2002).

1.4 Functions of Hsp70

Hsp70s have a broad range of cellular functions; they assist in folding, assembly of nascent proteins, prevention of protein aggregates formation, refolding, degradation, membrane translocation, apoptosis, and cellular protection. In the cellular milieu, Hsp70 proteins can identify and carry out the control of misfolded proteins and the post-translational folding of nascent proteins through their exposed hydrophobic core without any interaction with folded sides, then provide appropriate conditions for refolding proteins into their native conformations (Alderson *et al.*, 2016). Moreover, they assist in translocation of organelle-targeted proteins through the membranes, interact with specific native proteins and reform their activities, stabilities and oligomeric conditions specifically in some cellular stress conditions (Mayer, 2013). Hsp70s have an important role in proteostasis, and they have become a favorable anti-bacterial target and also are used in the drug targeted treatment for cancer (Ung *et al.*, 2013).

Hsp70s locate in different organelles in eukaryotes and have unique roles in these compartments. For example, SSC1 gene is a mitochondrial Hsp70 in *Saccharomyces cerevisiae*, and has a critical role for protein transportation across the inner membrane and folding of mitochondrial proteins (Azem *et al.*, 1997). In endoplasmic reticulum, Hsp70s refold or degrade misfolded proteins (Mori *et al.*, 1996). Furthermore, Hsp70s have significant role in programmed cell death and immune response. In programmed cell death, apoptotic proteins inhibit the caspase signalling pathway by binding apoptotic protease activating factor molecule (Gober *et al.*, 2005; Jäättelä *et al.*, 1998). When considering the immune response, Hsp70s may prevent inflammatory damage (Borges *et al.*, 2012). Dysregulation and mutations in Hsp70s are implicated in immunological diseases, neurodegenerative diseases, and cardiovascular diseases. Besides, neuronal cells suffer from the formation of large amount of protein aggregation in some diseases such as amyotrophic lateral sclerosis, Alexander's disease, Alzheimer's disease, Huntington's disease, Parkinson's disease, Wilson's disease, and prion-related human syndromes (Esser *et al.*, 2004).

1.5 Molecular Mechanism of Hsp70

Substrate binding domain of Hsp70s binds to hydrophobic substrates that are short amino acid stretches in *de novo* or partially unfolded protein sequences, while nucleotide binding domain (also referred as ATPase domain) controls the affinity of SBD for substrates with an ATP-dependent fashion through the linker sequence, which results in the formation of different conformational states. Binding of substrates to SBD also increases the ATP hydrolysis rate in NBD, indicating an allosteric communication between the Hsp70 domains (Bukau and Horwich, 1998). The nucleotide binding domain (NBD) of Hsp70 (in ATP and ADP bound forms) have two main lobes. These domains are divided into upper-lower parts and right-left part. The lower and upper parts are named as A and B, respectively, and the right and left parts are named as I and II, respectively. Thus, these subdomains called as IA (residues 1-37 and 120-171), IIA (residues 172-227 and 311-368), IB (residues 38-119) and IIB (residues 228-310). IB and IIB are in communication with adenosine and deoxyribose moieties (Figure 1.2). These subdomains are classified by a hydrophilic nucleotide binding site (Mayer, 2013).

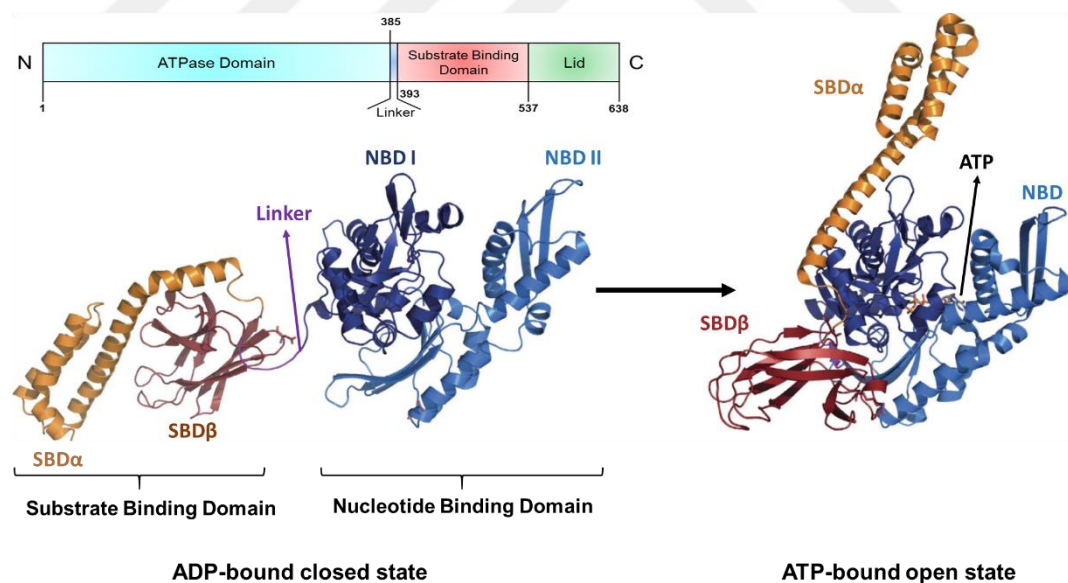


Figure 1.2: Crystal Structure of DnaK (Hsp70 homolog) in the ADP-bound closed conformation (left, PDB ID 2KHO) and in the ATP-bound open conformation (right, 4B9Q15) (Adapted from Kityk *et al.*, 2015).

E. coli Hsp70 (DnaK) has a hydrophobic region between IA and IIA subdomains, IB and IIB subdomains control the accessibility of the nucleotide binding side. “A” subdomains and “B” subdomains are bound with flexible hinges (Chiappori *et al.*,

2012). These subdomains are complexed with a Mg^{2+} and two K^+ ions. NBD binds and hydrolyses ATP to ADP. In the ATP-bound state, Hsp70s have low affinity for substrate. When ATP binds to NBD, it hydrolyses ATP to ADP and increases the substrate binding affinity. The J-domain is absolutely necessary to increase ATP hydrolysis with Hsp70 (Malinverni *et al.*, 2017). Conversely, binding of substrate stimulates ATP hydrolysis via an allosteric mechanism (Mayer, 2013).

The substrate binding domain (SBD) has a conserved sequence in Hsp70 proteins. SBD comprises of two parts which are α -helical lid subdomain and 10 kDa β -sandwich subdomain (Figure 1.3). The α -helical lid acts as a cover for SBD over the polypeptide binding state. The β -sandwich (peptide-binding cleft) binds substrates with a hydrophobic groove for polypeptide binding and it is enriched in hydrophobic amino acids such as Leu, Val and Ile (Rüdiger *et al.*, 1997). ATP-bound state encourages the flexibility between α -helical lid and β -sandwich. Inversely, polypeptide binding in the SBD increases the ATP hydrolysis rate (Young, 2010).

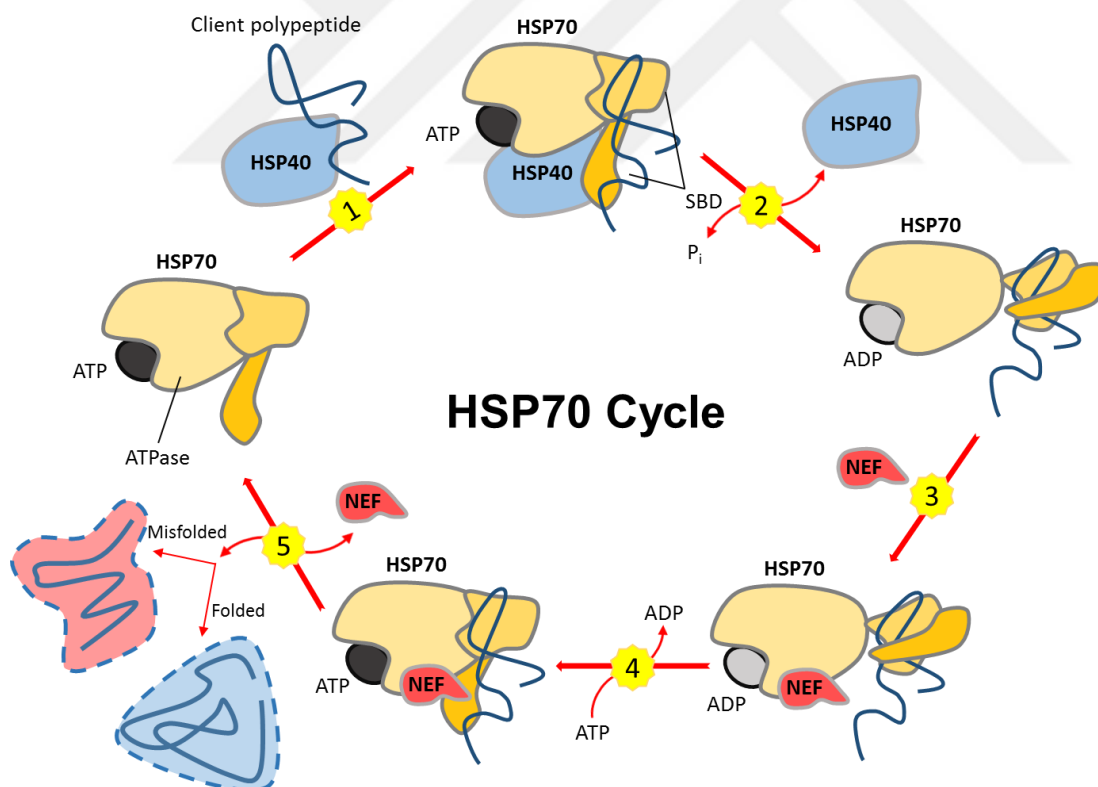


Figure 1.3: Hsp70 machinery. (Adapted from Brehme and Voisine, 2016). ATP is shown as dark grey, ADP is shown as light grey, substrate is shown as blue line, NBD is shown as light orange, SBD and lid are shown as orange, Hsp40 is shown as light blue, and Nucleotide exchange factor (NEF) is shown as red.

Hsp40 starts the cycle of Hsp70 directly by binding to unfolded client polypeptide from their hydrophobic groove. Then Hsp40 interacts with the substrate binding domain (SBD) of ATP-bound Hsp70s for the delivery of substrate. At the ATP-bound state of Hsp70, lid of SBD becomes flexible and peptide binding site opens. Hsp40 increases the ATPase rate of Hsp70 and results in the hydrolysis of ATP to ADP. ADP-bound Hsp70 forms a lid-closed structure and results in a more stable interaction with substrate than that of ATP-bound state. Nucleotide exchange factor (NEF) interacts with ADP-bound and nucleotide-free states of Hsp70 and switches ADP to ATP. This switch leads to the open structure, which releases the client polypeptide from Hsp70. Then substrate and NEF are released as a result of conformational rearrangement of NBD. At the end of the cycle, there are two different possibilities; client polypeptide successfully acquires its properly folded native state or folding process fails, resulting in the repeat of Hsp70 cycle for the unfolded substrate (Figure 1.3) (Brehme and Voisine, 2016; Mayer and Bukau, 2005).

1.6 Structure of Hsp70

From the structural viewpoint the Hsp70 family members include two main domains including a highly conserved 44 kDa N-terminal nucleotide binding domain (NBD) (PDB ID: 1DKG) and a variable 25 kDa the substrate binding domain (SBD) which is located at the C-terminal (PDB ID: 1DKX) (Uchida and Kanemori, 2018). These two domains are connected to each other with highly conserved hydrophobic linker (GDVKDVLLL) which has 6-10 amino acids (Kityk *et al.*, 2012). That hydrophobic linker plays a critical role in allosteric mechanism of Hsp70. Structural domains of DnaK, which is an *Escherichia coli* homolog of Hsp70, are represented in Figure 1.2. SBD of *E. coli* Hsp70 were observed by X-ray crystallographic studies with isolated SBD of DnaK in complexed with heptapeptide substrate (NRLLLTG) (Zhu *et al.*, 1996). The non-nucleotide form of intact bovine Hsc70, which has closed conformation and lacks 10 kDa C-terminal oligomerization domain, was the first X-ray crystallography study performed by Jiang *et al.*, (2006). Based on the Nuclear Magnetic Resonance (NMR) studies, undocked three-dimensional structure of DnaK has been shown to be in complex with peptide and ADP (Bertelsen *et al.*, 2009). To demonstrate the detailed properties of the allosteric landscape of the bacterial Hsp70,

IM-MS and DEER techniques were used by Lai *et al.*, (2017). These previous studies ensured information about the structures of NBD and SBD in different ligand forms.

1.7 Dynamic Studies of Hsp70

Recent structural studies enlightened the association between NBD and SBD of Hsp70s. DnaK regulates the allosteric interaction between NBD and SBD. To probe the allosteric transitions of DnaK, the wild-type and mutant was characterized at the nucleotide-induced absorbance changes in the vibrational spectrum and to determine the conformation sensitive absorption bands, three mutants were used; SBD α -deficient, NBD only, and full-length T199A mutant (Chang *et al.*, 2010). Mutant and wild-type proteins were analyzed with time-resolved infrared difference spectroscopy unified with the use of caged-nucleotides. This study shows that binding of ATP supports the conformational changes of the peptide binding domains in its subdomains and this conformational rearrangement reduces the affinity of DnaK for peptide substrates (Rodriguez *et al.*, 2008).

It is difficult to study with the substrate-free SBD, due to the tendency of binding nearly any free substrate. The substrate-free state and substrate-bound conformations were used for NMR chemical shift and hydrogen-deuterium exchange (HDX) analysis. According to the results, substrate-unbound state and substrate-bound state are almost similar (Swain *et al.*, 2006).

Harrison *et al.* (2009) focused on the three-dimensional construction of the ATPase domain of DnaK in complex with GrpE and the role of GrpE interactions of influencing DnaK-peptide. Nucleotide-bound Hsp70 structure is almost same with DnaK when GrpE binds to nucleotide-free NBD. They studied with ATPase domain, full-length GrpE and mutant form of GrpE (G122D). Results show that two helices extend through the GrpE dimer, suggesting that GrpE may have a role in peptide release from DnaK.

The closed-conformation of Hsp70 occurs upon ATP hydrolysis, α -helical lid is closed onto β -sandwich and peptide dissociation rates decreases. Peptides interact with the hydrophobic groove of Hsp70 (Mayer, 2013).

Although the majority of Hsp70 studies focused on the investigation of the closed conformation of Hsp70s, some groups studied on the open conformation of Hsp70s

(Kityk *et al.*, 2015; Qi *et al.*, 2013). When the structure of the open conformation of Hsp70s are investigated, it is observed that α -helical lid and β -sandwich of SBD are separated from each other and docked to a different region of NBD. Interaction between β -sandwich and NBD displays the allosteric regulation. This interdomain communication shows that the linker attaches to the hydrophobic groove of the hydrophobic binding domain and β -sandwich docks with NBD. Then, α -helical lid is closed onto the NBD (Kityk *et al.*, 2012). It also suggests that stabilizing the closed conformation does not initiate signal for ATP hydrolysis (Kityk *et al.*, 2015). In the open conformation of Hsp70, when nucleotide binding groove is closed, NBD-IA and NBD-IIA open and the opened groove interacts with interdomain linker (Mayer, 2013).

To investigate the interdomain communication mechanism, Swain *et al.* (2007) studied with two different constructs of DnaK. Both residues contain NBD, which are DnaK₃₈₈ and DnaK₃₉₂. DnaK₃₉₂ has a conserved hydrophobic ³⁸⁹VLLL³⁹² sequence of the interdomain linker, while DnaK₃₈₈ lacks this linker sequence. They show that the DnaK₃₉₂ is almost similar to substrate-stimulated ATPase rates of full-length of DnaK and they are highly pH-sensitive. However, DnaK₃₈₈ and unstimulated full-length of DnaK are insensitive to pH (Swain *et al.*, 2007).

To prove the detailed properties of the allosteric landscape of DnaK, characterization methods are applied which are IM-MS and DEER (Lai *et al.*, 2017). These characterization methods explained how the chaperone's conformational ensembles shift in response to different ligands (ATP, ADP/substrate, and ATP/ substrate). These techniques were detected the allosterically active state of DnaK (ATP/substrate-bound) which is a partially docked discrete intermediate.

1.7.1 Secondary structure analysis using circular dichroism

Circular dichroism (CD) spectra measures the differential absorbance of left and right-handed circularly polarized light. CD is a very sensitive and rapid determination technique to analyze the different structural types; the secondary and tertiary structure of proteins and polypeptides. Phenylalanine, tyrosine, tryptophan and disulphide bonds in the tertiary structure of proteins are measured in the near-UV. In addition, secondary structure of proteins can be determined as α -helix, β -sheet, polyproline and irregular, which are measured in the far-UV. A random coil is the polymer

conformation in which the monomer subunits are randomly oriented but still connected to adjacent units. At the spectrum, α -helix structured proteins have a positive band at ~ 190 nm and two negative bands at 222 and 208 nm. β -sheet structured proteins have a positive band between 195-200 nm and a negative band between 210-220 nm (Corrêa and Ramos, 2009). Representative graph of a secondary structure α -helix and β -sheet proteins in the far-UV is given in Figure 1.4.

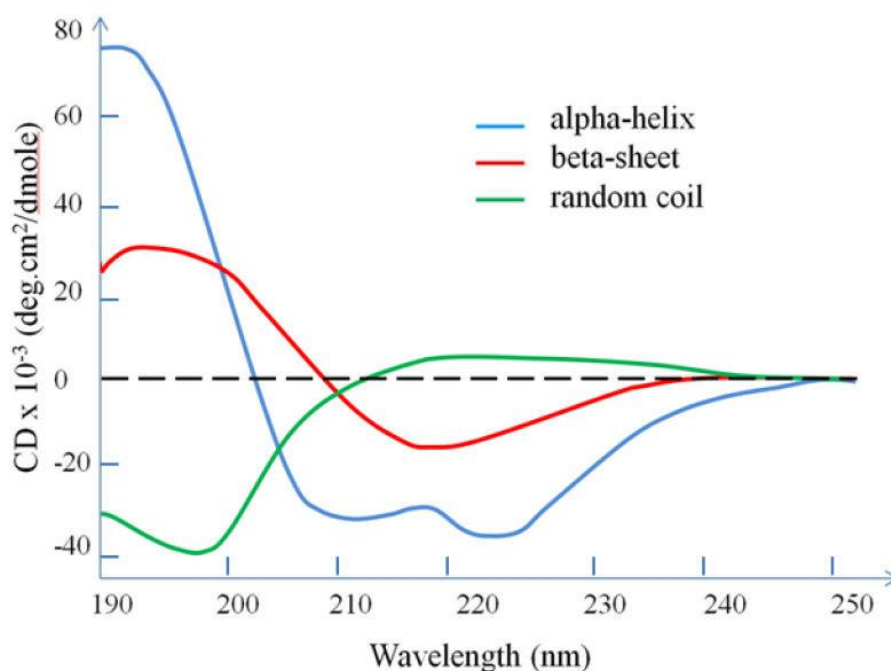


Figure 1.4: Secondary structure representation of α -helix, β -sheet and random coil polypeptide chain (Taken from Wei, et al. 2014).

1.7.2 Ion-mobility spectrometry

Native mass spectrometry is a biophysical technique which sprays the biological analytes under native conditions depending on electrospray ionization. Native MS is used in structural biology and it gives information such as, binding partners, protein dynamics, and protein complex topology. Accordingly, it is important to control the pH and ionic strength parameters to sustain the native folded state of the analytes in the solvent (Leney and Heck, 2017).

Ion-mobility spectrometry (IMS) is a prevalently used and the most successful technique to separate and identify small and large biological compounds depending on their size, mass, shape and charge (Cumeras *et al.*, 2016). IMS distinguishes structural differences that the MS technique cannot distinguish on its own. IMS characterizes flexibility and folding mechanisms to gain information about the conformational

dynamics of a system (Lanucara *et al.*, 2014). Various IMS platforms are available based on applied electric field and types of buffer gas, such as drift time (DT), travelling wave (TW) and differential mobility. In this project, drift time is used providing a homogeneous linear electric field which allows the determination of collision cross section of molecules (Zheng *et al.*, 2017).

IMS consists of four essential region; a detector, a drift tube, an ion source region and an ion gate. Ion gate is used to inject ions from the ion source region and delivers them to drift tube. Ions move through the tube and reach the detector under the influence of electric fields creating a signal (Ewing *et al.*, 2001). Ions are driven through a gas-filled chamber under the influence of an electric field. They collide with nitrogen atoms and separated by their size and charge. Larger molecules collide more frequently with the inert ion increasing their drift time more than compact ions (Ben-Nissan and Sharon, 2018). The number of collisions depends on the size of molecules and offers a way to calculate collision cross section (CCS) of molecules that gives an idea regarding three-dimensional shape.

Knapman *et al.*, (2013) are used ESI-IMS-MS technique to probe the conformational characteristics *holo*- and *apo*-cytochrome c. Their results demonstrated mass spectra acquired at pH 7, pH 4 and pH 2 for both *holo*-cytochrome c (12,355 Da, including the haem ligand) and *apo*-cytochrome c (11,702 Da). *Holo*-protein indicated ESI-MS behavior similar to native-like, folded protein. Moreover, four charge state ions (5+ to 8+) can be seen at neutral pH. Higher charge state ions are monitored at lower pH values, showing acid-unfolded structure of the protein (5+ to 17+) also folded conformers are raised from at lower charge states, it can still be observed. On the contrary, the distribution observed for the *holo*-protein at pH 2 is parallel to all three pH values for *apo*-protein and it supports the presence of widened, unopened conformic species even at neutral pH.

1.8 Aim of This Study

Proteins exist as dynamic entities, which possess a population of different conformational structures. Their function depends on the existence of these conformational populations. The current study has been carried out to probe the arrangement of the conformational ensembles of Hsp70 and to understand the most abundant population. One previous study performed by Swain *et al.*, (2007)

demonstrated the differences between DnaK₃₉₂ and DnaK₃₈₈. The presence of linker present in DnaK₃₉₂ conformation, mimics the active form of the ATPase domain. We think that these differences can be effective at the equilibrium state of conformational distribution in populations. To understand the phenomenon behind conformational diversity in DnaK₃₉₂ and DnaK₃₈₈, native MS and ion-mobility mass spectrometry (IM-MS).experiments were applied in this project.



2. MATERIALS AND METHODS

2.1 Materials

2.1.1 Laboratory equipments

The equipments used in the experiments are given in Appendix A.

2.1.2 Chemicals and enzymes

The chemicals and enzymes used in the experiments are given in Appendix B.

2.1.3 Commercial kits

Invitrogen PureLink[®] Quick Plasmid Miniprep Kits (Invitrogen, ABD) used as were the commercial kits used in the experiments.

2.1.4 Bacterial strains

In this study, *Escherichia coli* XL-1 Blue strain [recA1 endA1 gyrA96 thi-1 hsdR17 supE44 relA1 lac F' proAB lacIqZΔM15 Tn10 (Tetr)] and *Escherichia coli* BB1553 strain [MC4100 _dnaK52::cmR sidB1] (Stratagene) bacterial strains were used.

2.1.5 Buffer and solutions

Preparation of buffer and solutions are explained in Appendix C.

2.2 Methods

2.2.1 Preperation of DH5α competent cells

Competent *Escherchia coli* - DH5α was prepared for chemical transformation according to Inoue method (Sambrook and Russell, 2006). Briefly, cells were taken from glycerol stock and spread onto Luria-Bertani (LB) agar plate, then it was incubated for growth overnight at 37°C. After 16 hours, one colony was taken from the plate with a tip and it was directly put in falcon which was containing 5 mL LB medium. Then, it was incubated overnight at 37°C in orbital shaker at 180 rpm. The

following day, 5 mL of overnight culture solution was added in 100 mL LB medium and it was incubated at 37°C in orbital shaker at 180 rpm. Optical density was measured until the OD₆₀₀ = 0.8-1.0 was achieved. Then, bacteria were transferred to sterile 50 mL ultracentrifuge falcon tubes and incubated on ice for 10 minutes. The cells were centrifuged at 1600xg for 7 minutes at 4°C. The supernatant was discarded and pellet was resuspended in 32 mL ice-cold Inoue buffer, incubated 5 minutes on ice. Then it was centrifuged at 1600xg for 7 minutes at 4°C. The supernatant was discarded and pellet was resuspended in 8 mL ice-cold Inoue buffer (55 mM MnCl₂, 10 mM PIPES (0.5M, pH 6.7), 15 mM CaCl₂, 250 mM KCl). 1 M DMSO was added into the sample and it was incubated in ice for 10 minutes. Finally, the cells were divided into 50 µL aliquotes in 0.75 mL sterile microcentrifuge tubes and stored at -80°C for further use.

2.2.2 Plasmid transformation of competent cells

The competent cells were taken from -80°C and were thawed on ice. 2 µL of purified plasmid DNA (pMS-DnaK) (~153.0 ng/µl) was added into 20 µL of competent cells and the microcentrifuge tube containing the cells was incubated on ice for 30 minutes. The cells were heated at 42°C for 45 seconds and placed on ice for 2 minutes. 250 µL LB was added and it was incubated for 1 hour at 37°C in orbital shaker at 225 rpm. Cells were spread on LB agar plate containing the appropriate antibiotic (ampicillin) and the plate was incubated at 37°C overnight for 16 hours for allowing colonies to form.

2.2.3 Plasmid DNA preparation

Single colony of *E. coli* - DH5α cells from overnight grown plate was taken into 7 mL LB medium containing the appropriate antibiotic (ampicillin). The next day after incubation, bacteria were transferred to sterile ultracentrifuge tubes and centrifuged at 4500xg for 15 minutes at 4°C. Plasmid DNA isolation was performed using Invitrogen PureLink[®] Quick Plasmid Miniprep Kits (Invitrogen, ABD) according to manufacturer's instructions. Briefly, pellet was taken from -80°C and it was thawed. Bacterial cell pellet was resuspended with R3 Buffer, which contains RNase A. Then, cells were lysed with L7 Buffer and incubated room temperature for 5 minutes. After 5 minutes, N4 Buffer was added for precipitation and centrifuged. The supernatant was transferred to spin column and then centrifuged. After that, W9 Buffer was added for

washing and the sample was centrifuged. Then, spin column was placed in a clean 1.5 mL recovery tube and TE Buffer was added. The sample was incubated 1 minute at room temperature. Finally, to elute DNA, TE Buffer was added to the center of the column and incubated 1 minute at room temperature, then it centrifuged. Plasmid concentrations were determined with Thermo Scientific NanoDrop 2000 spectrophotometer at 280 nm. Isolated plasmid DNA was stored at -20°C.

2.2.4 Preparation of BB1553 competent cells

Competent *E. coli* – BB1553 (Δ dnaK) was prepared for transformation by Inoue method. *E. coli* – BB1553 cell was taken from stock and spread onto LB agar plate, then it was incubated for growth overnight at 37°C. After 16 hours, single colony was taken from the plate with a tip and it was directly put in falcon which was containing 10 mL LB medium. Then, it was incubated overnight at 37°C in orbital shaker at 225 rpm. The following day, 10 mL of overnight culture solution was added in 100 mL LB medium and it was incubated at 37°C in orbital shaker at 225 rpm. Optical density was measured until it was reached $OD_{600} = 0.6$. After, bacteria were transferred to sterile 50 mL ultracentrifuge falcon tubes and it was incubated on ice for 10 minutes. The cells were centrifuged at 2300xg for 10 minutes at 4°C. The supernatant was discarded and pellet was resuspended in 32 mL ice-cold Inoue buffer, the cells were incubated 5 minutes on ice. Then it was centrifuged at 2300xg for 10 minutes at 4°C. The supernatant was discarded and pellet was resuspended in 8 mL ice-cold Inoue buffer and added 600 μ L DMSO. It was incubated on ice for 10 minutes. Finally, the cells were divided into 50 μ L aliquots in 0.75 mL sterile microcentrifuge tubes and they were stored at -80°C.

2.2.5 Plasmid transformation of BB1553 competent cells

The competent cells were taken from -80°C and thawed on ice. 1.5 μ L of purified plasmid DNA (pMS-DnaK) was added into 50 μ L of competent cells and the cells were incubated on ice for 30 minutes. Subsequently, the cells were heated at 42°C for 45 seconds and put on ice for 2 minutes. 250 μ L LB was added and it was incubated for 1 hour at 37°C in orbital shaker at 225 rpm. Cells were spread on LB agar plate containing the appropriate antibiotic (ampicillin) and the plate was incubated at 37°C overnight for 16 hours.

2.2.6 Growth of the transformed BB1553 cells

Single colony of *E. coli* – BB1553 cells from overnight grown plate was taken into 100 mL LB medium containing the appropriate antibiotic (ampicillin and chloramphenicol). Then, it was incubated overnight at 30°C in orbital shaker at 200 rpm. The next day after incubation, 100 mL of overnight culture solution was added in 4 L LB medium and it was incubated at 30°C in orbital shaker at 200 rpm. Optical density was measured until it was reached $OD_{600} = 0.8-1$. Then, 1 mL of culture was separated for control and the 0.2 mM IPTG was added. It was incubated for 4 hours at 30°C in orbital shaker 200 rpm. After, bacteria were transferred to sterile ultracentrifuge tubes and it was centrifuged at 4500xg for 15 minutes at 4°C.

2.2.7 Preparation of cell extract

E. coli – BB1553 cells were taken from -80°C and thawed. Total protein was extracted with an appropriate amount of resuspension buffer, lysozyme (0.2 mg/ml), DNase I (0.15 mg/ml) and protease inhibitors cocktail tablet. Cells were incubated on ice for 30 minutes with the mixture. Then, sonication was applied to cells 7 minutes roughly 10 times burst and 20 second rest on ice. Finally, the cells were centrifuged at 16000xg for 45 minutes at 4°C. The supernatant was collected, filtered with 0.22 µm syringe filter and dialyzed with a 30 mm dialysis pack with anion binding buffer for further purification experiments.

2.2.8 Control of induction

Induced and uninduced protein samples were extracted with appropriate amount of resuspension buffer, lysozyme and PMSF. After samples were incubated on ice for 30 minutes with the mixture, 15 µL of samples were mixed with 4X Laemmli for SDS-PAGE analysis.

2.2.9 DnaK purification with DEAE Sepharose FF column

DEAE Sepharose FF is an anion exchanger based on the well-established Sepharose Fast Flow ion exchange platform. All anion exchange chromatography trials were performed via GE Healthcare AKTA Avant Purification System. 1 ml of HiTrap DEAE Sepharose FF column was used for separating DnaK proteins from positively charged proteins. The content of starting and elution buffers used for purification is given below. 1 ml of HiTrap DEAE Sepharose FF column had been cleaned with 0.5

M NaOH, 20% ethanol and ddH₂O, respectively. Then HiTrap DEAE Sepharose FF column was equilibrated by 20 mM Tris-HCl, 1 mM EDTA, pH 7.4 binding buffer with 1 ml/min flow rate until the conductivity became more than 190 mS. 25 ml DnaK₃₉₂ sample was injected into the system via 10 ml volume of injector. The column was washed with 1 ml/min flow rate 10 column volume and the sample was loaded onto the column with 1.0 ml/min flow rate with starting buffer. Elution step was performed as linear gradient. The eluted fractions were collected in 2 ml microcentrifuge tubes and monitored by SDS-PAGE. Subsequently, DnaK eluents were pooled and dialyzed with a 30 mm dialysis pack with HMK binding buffer. Dialyzed protein sample was loaded onto ATP-agarose column.

Starting buffer: 20 mM Tris-HCl, 1 mM EDTA, pH 7.4

Elution buffer: 20 mM Tris-HCl, 1 mM EDTA, 1 M NaCl, pH 7.4

2.2.10 DnaK purification with ATP-agarose column

ATP-agarose is an affinity column, which is composed of ATP-agarose beads. All affinity chromatography experiments were performed via GE Healthcare AKTA Start Purification System. ATP-agarose column was used for separating purified DnaK proteins. The content of wash, starting and elution buffers used for purification are given below. ATP-agarose column had been cleaned with 10 column volumes of washing buffer 1 to prevent cross contamination. Then, ATP-agarose column was equilibrated by HMK binding buffer with 1 ml/min flow rate until the conductivity became more than 190 mS. After that, concentrated protein sample was loaded onto the ATP-agarose column. The column was washed with 4 column volumes of washing buffer 2 for removing nonspecifically bound proteins. The ATP-agarose column was re-equilibrated with 3 column volumes of HMK binding buffer with 1 ml/min flow rate. Lastly, DnaK proteins were eluted with HEK elution buffer. Elution step was performed as linear gradient. The fractions were collected in 2 ml eppendorf tubes. Elution fractions were checked by SDS-PAGE.

Washing buffer 1: 10 mM EDTA, 100 mM KCl

HMK (Binding) buffer: 20 mM HEPES, 5 mM MgCl₂ and 100 mM KCl, pH 7.4

Washing buffer 2: HMK+ 2 M KCl

HEK (Elution) buffer: 20 mM HEPES, 10 mM EDTA and 100 mM KCl, pH 7.4

2.2.11 Column regeneration

ATP-agarose is an affinity column which includes ATP-agarose beads. ATP-agarose resin can be regenerate. ATP-agarose resin was washed with 20 column volumes of 50 mM Tris-HCl, 0.2 mM EDTA and 100 mM KCl, pH 8.2. ATP-agarose resin was incubated with 0.2 mM phosphoenol pyruvate, 10 units per ml of resin pyruvate kinase, 5 mM MgCl₂, 0.2 mM EDTA, 100 mM KCl and 50 mM Tris-HCl, pH 8.2 overnight at 2°C. Then, the resin was washed with 25 column volumes of 2 mM ATP and 2 M KCl. The resin was stored in HMK (Binding) buffer.

2.2.12 ATPase measurement

Steady-state ATPase activity of DnaK protein measurements were performed with an NADH-coupled ATPase assay is represented in Figure 2.1.

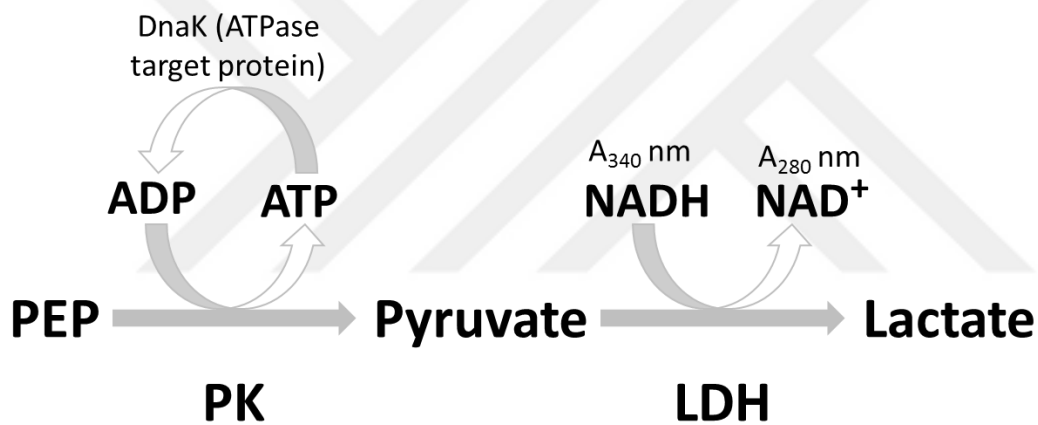


Figure 2.1: NADH-coupled ATPase assay.

As a principle, hydrolysis of ATP to ADP by DnaK. It causes to the conversion of phosphoenolpyruvate (PEP) generates pyruvate by pyruvate kinase (PK). In this reaction, lactate dehydrogenase (LDH) converts pyruvate to lactate. Then, NADH is oxidized to NAD⁺. ATPase activity was measured with decreasing of NADH at 340 nm for 30 minutes with 10 seconds interval and 5 minutes incubation, at 30°C by BMG LABTECH CLARIOstar[®] multi-mode microplate reader. This assay was prepared in the sterile 96-well plate with 200 µl sample reactions. Sample reactions contain 5X ATPase buffer (40 mM HEPES, 11 mM Mg(OAc)₂, 50 mM KCl), 5 mM DTT, 0.28 mM ATP, 1.02 mM PEP (in 1 X ATPase buffer pH 7.5), 0.2 mM β-NADH (in 1 X ATPase buffer pH 7.5), PK/LDH cocktail (9.94 U/ml PK-14.2 U/ml LDH), 1 µM protein as a final concentration. Reactions were applied with specific pH values as 5.5,

6.0, 6.5, 7.0, 7.5, 8.0, 8.5 5X ATPase buffer. An autohydrolysis reaction was performed with lacking the target protein to draw the correct slope. Protein concentrations were measured with Thermo Scientific NanoDrop 2000 spectrophotometer with an extinction coefficient of $18607 \text{ M}^{-1}\text{cm}^{-1}$ at 280 nm.

ATPase activity was calculated with the following formula using the obtained data. The autohydrolysis results were used as standard and the ATPase activity data graph was plotted according to that standard. The slope of the graph was found by linear regression. K_{path} is equal to 3,247 for each 200 μl sample volume.

$$\text{ATPase rate } [\text{min}^{-1}] = -\frac{dA_{340}}{dt} \left[\frac{OD}{\text{min}} \right] * K_{\text{path}}^{-1} * \text{moles}^{-1} \text{ATPase}$$

2.2.13 Circular dichroism (CD) measurements

Circular dichroism (CD) is a highly sensitive and rapid determination technique used for the analysis of the secondary and tertiary structure of proteins and polypeptides. In the far-UV, CD spectra is determined the secondary structure proteins as α -helix, β -sheet. At the spectrum, α -helix proteins have a positive band at ~ 190 nm and two negative bands at 222 and 208 nm. β -sheet proteins have a positive band between 195-200 nm and a negative band between 210-220 nm (Corrêa and Ramos, 2009). In this study, CD spectroscopy measurements were implemented by Jasco J-1500 Circular Dichroism Spectrophotometer (Jasco, Easton, MD). The CD scans were applied in the range of 200 nm and 250 nm using the 1 mm cuvette. The CD scan conditions were 1 nm step size, 1 nm bandwidth, 100 nm/min speed and 2 seconds response time at 25°C with approximately 10 μM purified protein. Purified protein samples were prepared in pH 7.0 HMK buffer.

2.2.14 Ion-mobility spectrometry

Ion-mobility spectrometry (IMS) is an analytical technique that can separate and identify compounds by their size, mass, shape and charge and it is the highly sensitive approach used for small and large biomolecule investigation (Cole *et al.*, 2015). Throughout the analysis, molecules are ionized via an electrospray source along the drift tube. After ionization, ions are transferred to the gas-filled chamber using an electric field. Drift time for ions to reach the detector is proportional to the size of the biomolecules. The greater biomolecules reach the detector later than smaller biomolecules.

All analytical analyzes were performed with Waters SYNAPT G2-Si HDMS (Waters, Manchester, U.S.). IMS measurements were applied with following instrument parameters; the transfer collision energy 2 V, sample cone 150 V, the capillary voltage of 2.3 kV, trap collision energies 4 V, trap DC bias 50 V, IMS gas flow 90 ml/min and helium cell gas flow 180 ml/min. The IM wave velocity ramp was set to 1200 m/s to 400 m/s and wave height was set to 40 V. All samples were taken into 100 mM ammonium acetate buffer via the 30K Amicon ultra centrifugal filter (Millipore, Billerica, MA). Buffer exchange was repeated 4 times in 5 different pH values which are 6.5, 7.0, 7.5, 8.0 and 8.5.



3. RESULTS

3.1 Analysis of Sequenced Data of Wild-type DnaK₃₉₂ and DnaK₃₈₈ in *E. coli*

DNA sequencing of wild-type DnaK₃₉₂ and DnaK₃₈₈ was performed by Iontek Biotechnology Incorporated Company and Macrogen. Analysis of sequence data was carried out by NCBI Standart Nucleotide BLAST. The alignment of sequence data is given in Appendix D. Full-length sequence of DnaK₆₃₈ was used as a template.

3.2 Expression of the Wild-type DnaK₃₉₂ and DnaK₃₈₈ in *E. coli*

NBD, which contains residues of wild-type DnaK₃₉₂ and DnaK₃₈₈ were overexpressed in *E. coli* BB1553 with the pMS-DnaK vector at 30°C. Low growth temperature was the optimum temperature for better cell survival. Proteins were overexpressed successfully with IPTG after 4 hours of induction. Induced and uninduced protein samples were extracted using lysozyme and PMSF. Further, samples were incubated on ice for 30 minutes with the mixture. Samples were mixed with 4X Laemmli for 12% SDS-PAGE analysis. SDS-PAGE result is demonstrated in Figure 3.1. As we expected, wild-type DnaK₃₉₂ and DnaK₃₈₈ were obtained at 42 kDa.

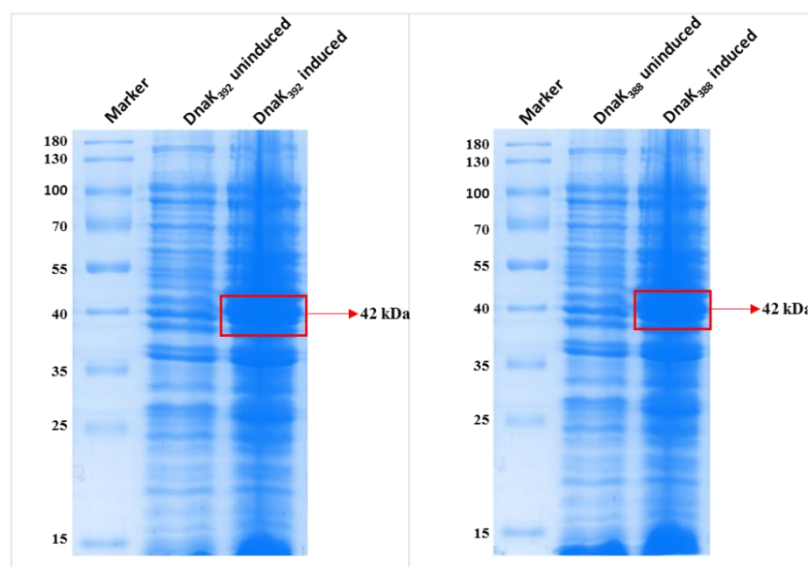


Figure 3.1: Induction control of wild type DnaK₃₉₂ and DnaK₃₈₈ by SDS-PAGE results.

3.3. Purification of the Wild-type DnaK₃₉₂ and DnaK₃₈₈ in *E. coli*

Centrifuged wild-type DnaK₃₉₂ and DnaK₃₈₈ cells were sonicated, centrifuged and supernatant was filtered. Then sample was concentrated with 30K Amicon ultra centrifugal filter (Millipore, Billerica, MA) with anion binding buffer for first step purification, which is an anion exchange purification approach. Afterwards, two consecutive purification methods, including anion exchange chromatography and affinity chromatography were followed. Representative chromatogram and SDS-PAGE results for wt DnaK₃₉₂ and wt DnaK₃₈₈ are shown in Figure 3.2 and Figure 3.3, respectively. Other replicates are represented in Appendix E.

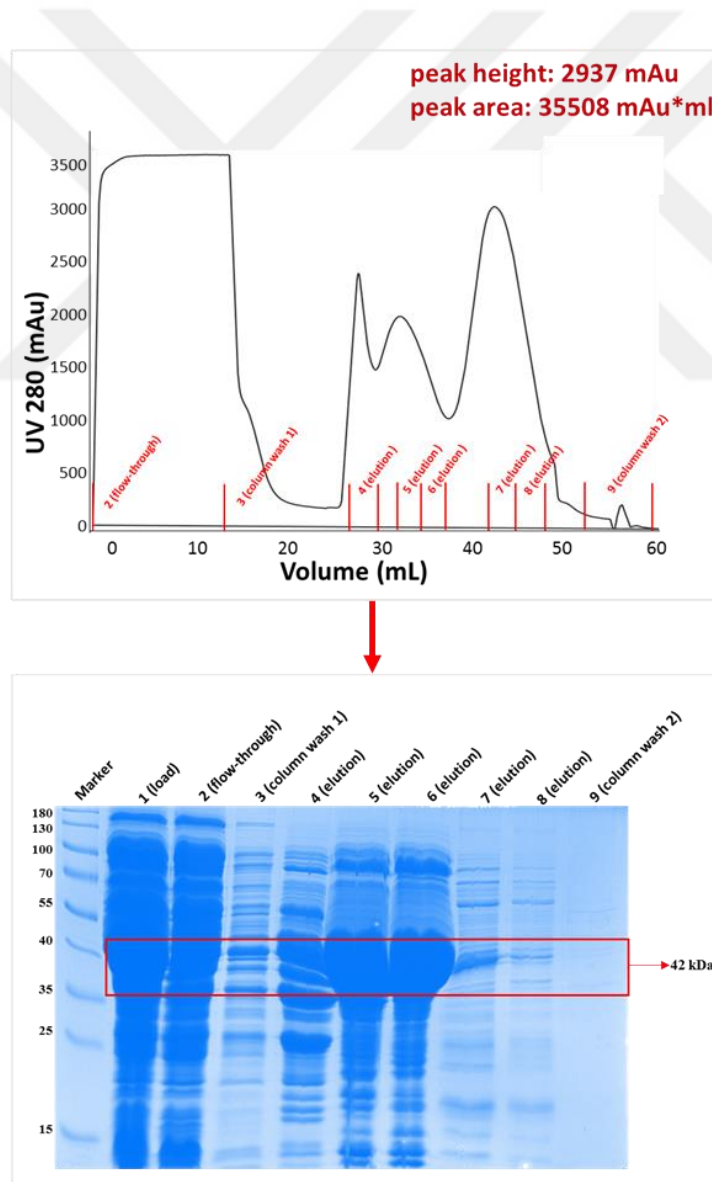


Figure 3.2: Anion Exchange Chromatogram of DnaK₃₉₂ (above) and Anion exchange chromatography fractions of DnaK₃₉₂ by SDS-PAGE (below).

Firstly, protein was purified with 20 mM Tris-HCl, 1 mM EDTA starting buffer and 20 mM Tris-HCl, 1 mM EDTA, 1 M NaCl elution buffer pH values are 7.4 using HiTrap DEAE Sepharose FF column. Anion exchange chromatography process was applied in bind-and-elute mode to bind target molecule and remove host cell proteins. Collected fractions, including flow-through, column wash 1 (before elution), elution and column wash 2 (after elution), were mixed with 4X Laemmli, and samples were loaded to 12% SDS-PAGE for further analysis. At the anion exchange chromatogram results, first peak contains host cells, other peaks are eluent peaks. As we expected at the SDS-PAGE result, wild-type DnaK₃₉₂ and DnaK₃₈₈ were obtained at 42 kDa.

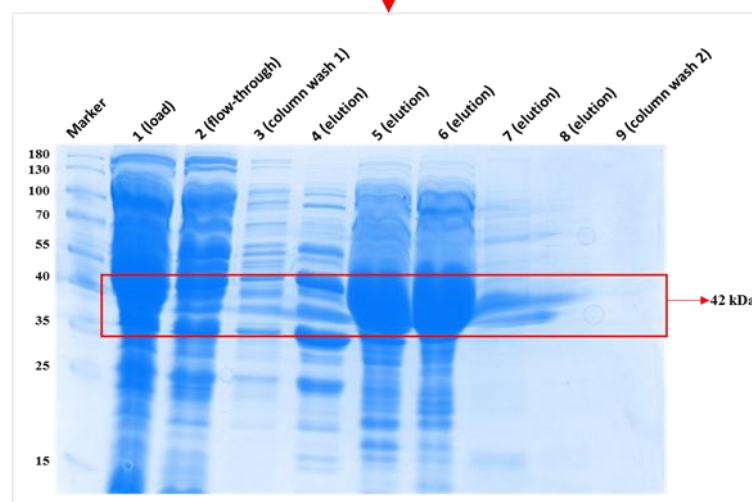
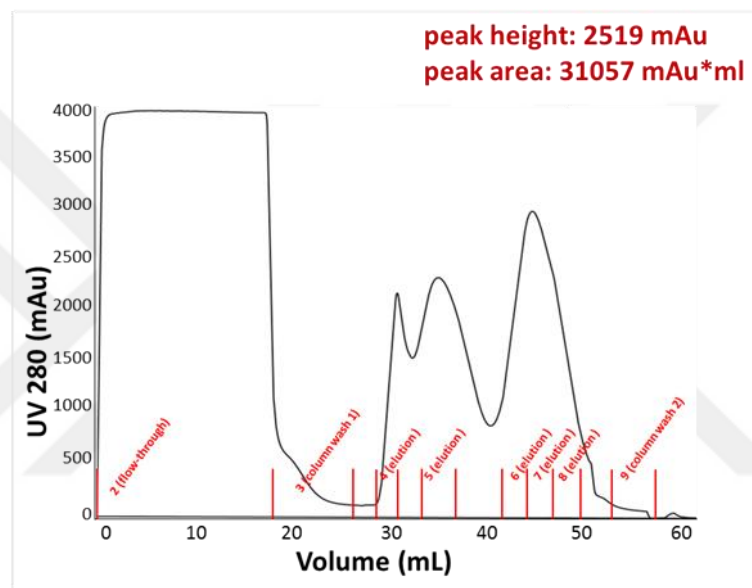


Figure 3.3: Anion Exchange Chromatogram of DnaK₃₈₈ (above) and Anion exchange chromatography fractions of DnaK₃₈₈ by SDS-PAGE (below).

As seen in the SDS-PAGE results, enriched DnaK₃₉₂ was detected. Peak fractions were dialyzed with 30 mm dialysis pack with HMK binding buffer for second step purification, which is an affinity purification approach. For affinity chromatography, ATP-agarose column was used and applied in the bind-and-elute mode. Dialyzed protein sample was loaded onto ATP-agarose column. Collected fractions, which were HMK+KCl (column wash), HMK (flow-through) and HEK (elution), were mixed with 4X Laemmli, and samples were loaded to 12% SDS-PAGE for analysis. Representative chromatogram and SDS-PAGE results are shown in Figure 3.4 and Figure 3.5. Other replicates are represented in Appendix E. As we expected at the SDS-PAGE result, DnaK was obtained at 42 kDa.

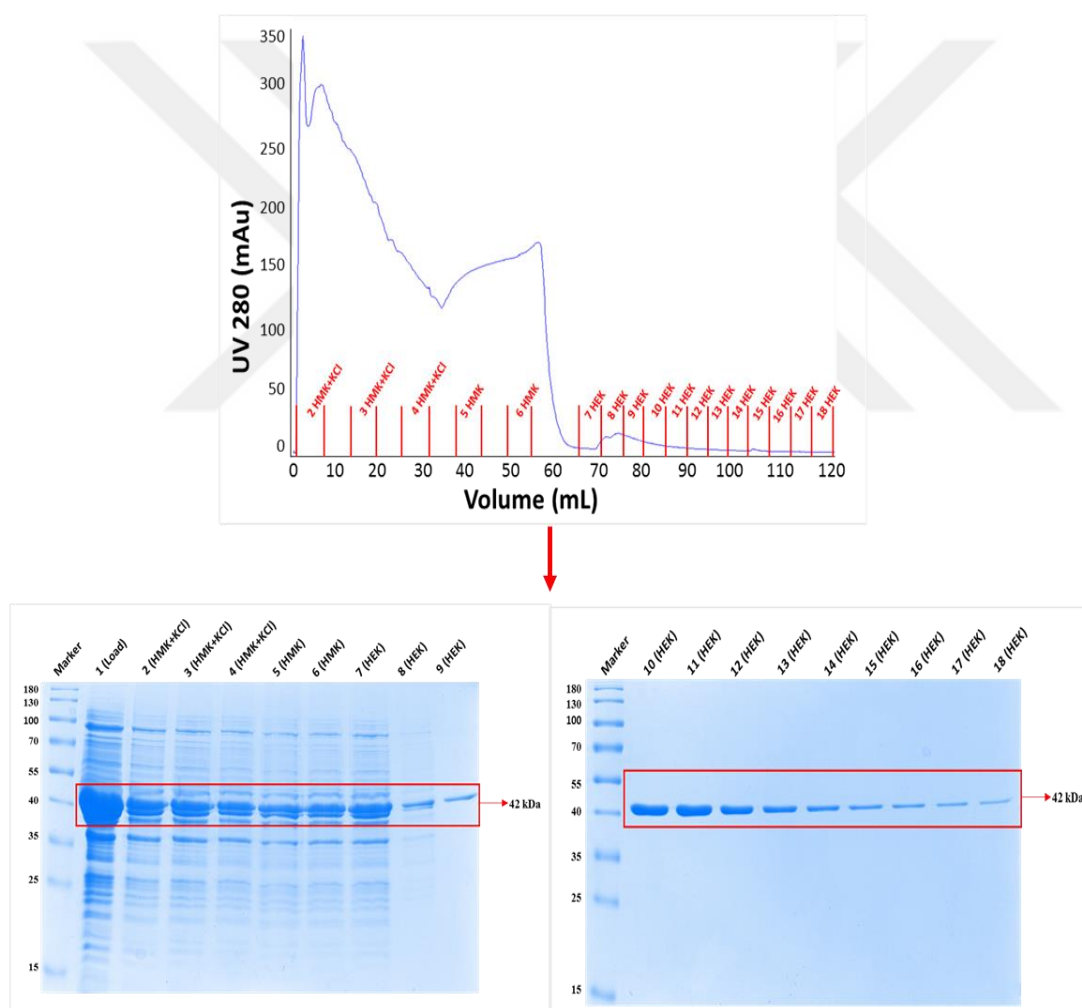


Figure 3.4: ATP Affinity Purification Chromatogram of DnaK₃₉₂ (above), DnaK₃₉₂ SDS-PAGE results from ATP affinity chromatography (below).

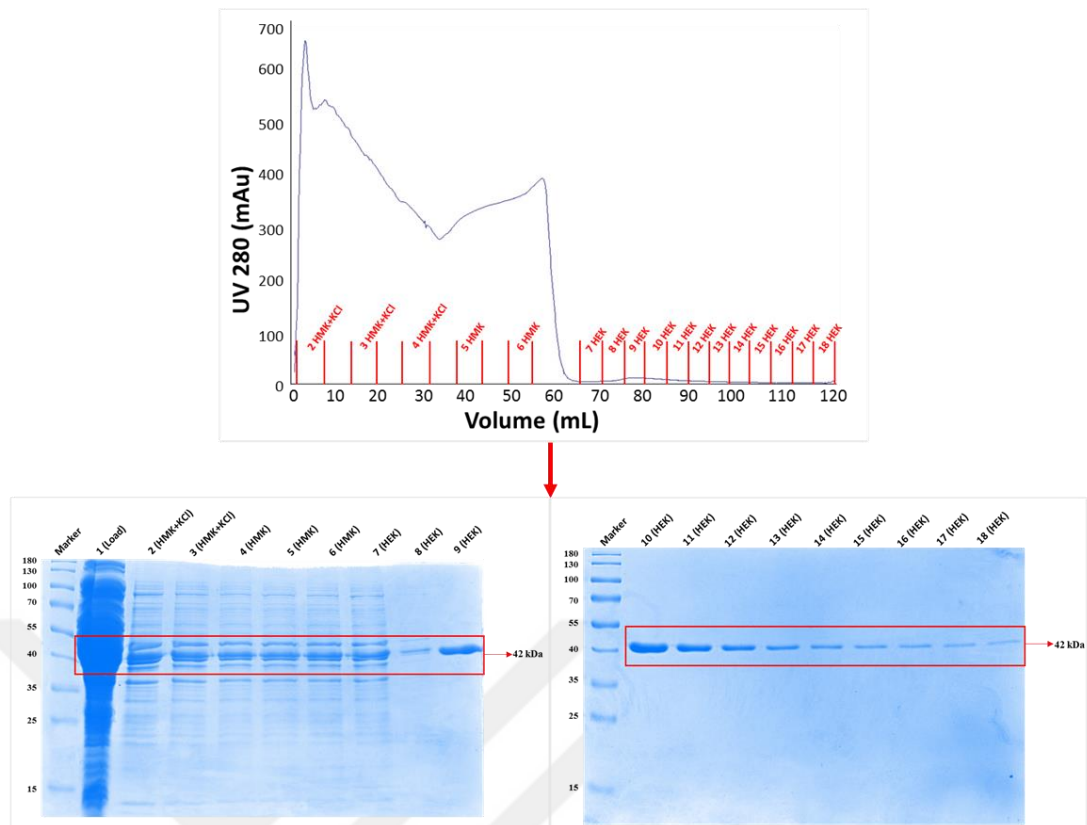


Figure 3.5: ATP Affinity Purification Chromatogram of DnaK₃₈₈ (above), DnaK₃₈₈ SDS-PAGE results from ATP affinity chromatography (below).

3.4 Result of Enzyme-coupled ATPase Assay

Enzyme-coupled ATPase assay was measured at different pH values between 5.5 and 8.5 to examine the effect on the pH-activity profile. Activity profile of kinetic measurements were performed for wild-type DnaK₃₉₂ and DnaK₃₈₈ to compare the previous result (Swain *et al.*, 2007). The concentration of DnaK₃₉₂ and DnaK₃₈₈ were measured with Thermo Scientific NanoDrop 2000 spectrophotometer with an extinction coefficient of $18607 \text{ M}^{-1}\text{cm}^{-1}$ at 280 nm. As mentioned in previous studies, the activity of DnaK₃₉₂ resembles full-length of DnaK. DnaK₃₈₈ lacks partial interdomain linker (³⁸⁸VLLL³⁹²), therefore it did not show stimulation with different pH values as observed for the full-length of DnaK (Swain *et al.*, 2007). DnaK₃₉₂ has maximum activity between pH 7.5 to 8.0 and ATPase profile of DnaK₃₉₂ has asymmetric bell-shape (Figure 3.6). On the contrary, DnaK₃₈₈ is more insensitive to pH than DnaK₃₉₂ and it lose of bell-shaped ATPase profile (Figure 3.7). In the absence of linker, ATPase activity rate is around basal pH values. DnaK₃₉₂ construct has 5 times higher ATPase activity around pH 7.5 than DnaK₃₈₈. As a conclusion, the linker is essential and sufficient for allosteric control of the ATPase domain by the SBD

(Swain *et al.*, 2007). The results of previous studies and our results are similar, in this case these proteins are functional and can be used for IMS experiments.

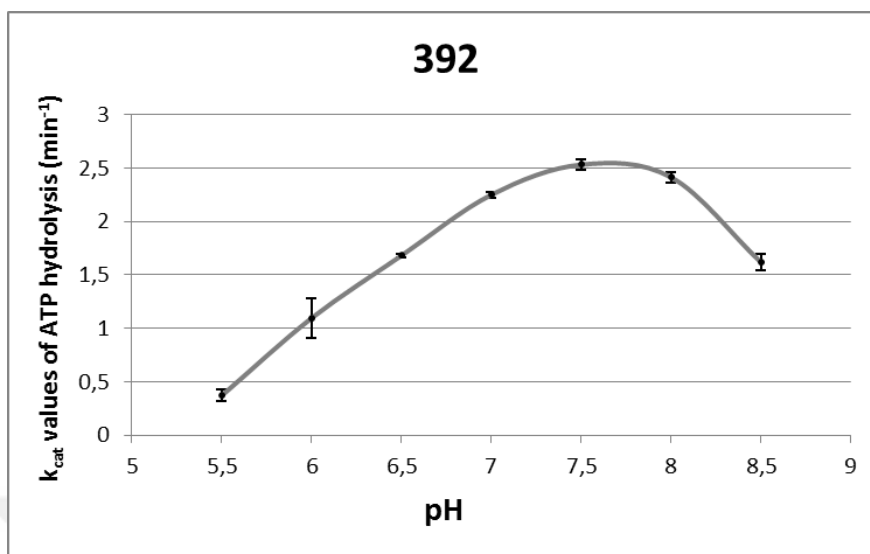


Figure 3.6: pH-dependent ATPase activity profiles of DnaK₃₉₂. Error bars on line represent standard deviation from 3 experiments.

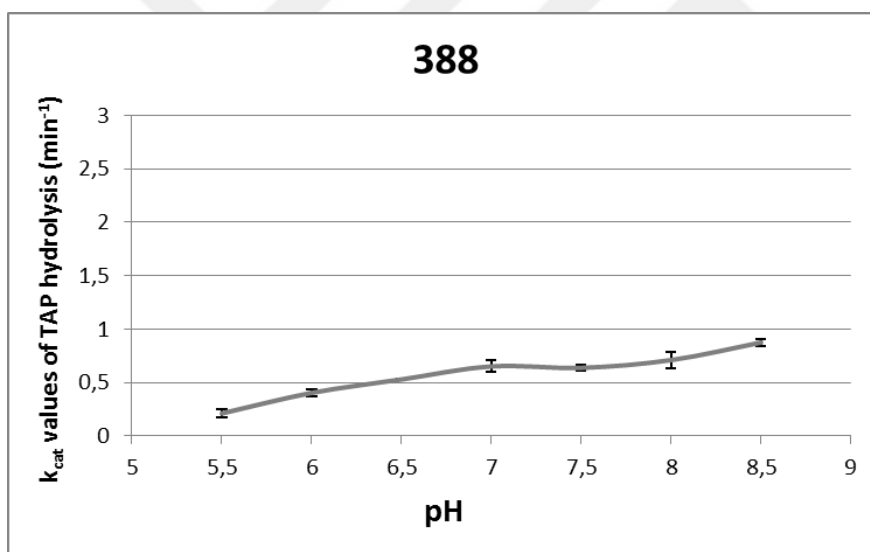


Figure 3.7: pH-dependent ATPase activity profiles of DnaK₃₈₈. Error bars on line represent standard deviation from 3 experiments.

3.5 Secondary Structure Analysis of DnaK₃₉₂ and DnaK₃₈₈

Secondary structure analyzes were performed using Jasco J-1500 Circular Dichroism Spectrophotometer (Jasco, Easton, MD). CD scans were conducted in wavelength range was set from 200 to 250 nm. These measurements were repeated 3 times for each samples.

Representative CD spectra graphs for DnaK₃₉₂ and DnaK₃₈₈ of wavelength at pH 7 are demonstrated in Figure 3.8 below. Other replicates are represented in Appendix E. As

seen in Figure 3.8, the structure of DnaK₃₉₂ and DnaK₃₈₈ has two negative bands at 222 and 208 nm, therefore these constructs have α -helical structure. A similar structure is observed in previous studies (Swain *et al.*, 2007). Since the CD spectra is not overlapped because of the different concentrations of DnaK₃₉₂ and DnaK₃₈₈ protein samples.

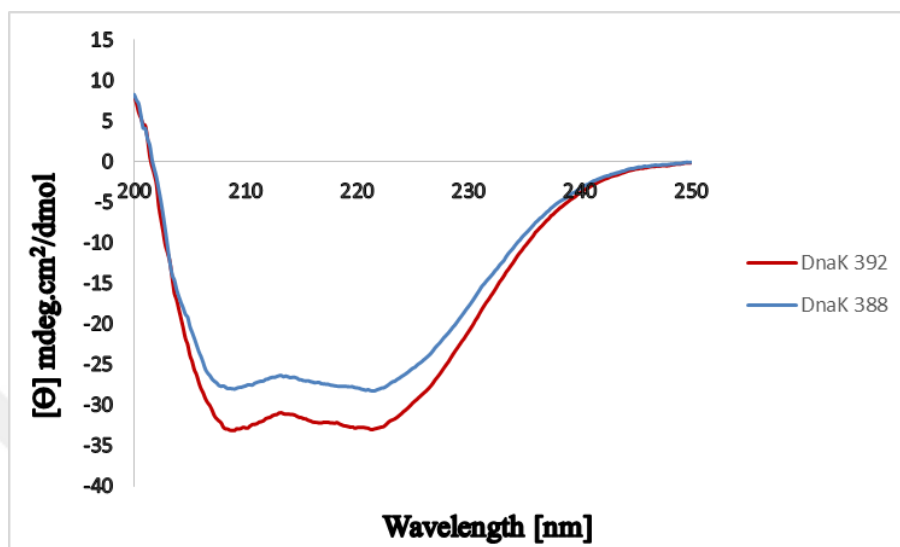


Figure 3.8: Circular Dichroism spectra results of DnaK₃₉₂ and DnaK₃₈₈.

3.6 Conformational analysis of DnaK₃₉₂ and DnaK₃₈₈ via Ion-Mobility Spectrometry

Ion-mobility spectrometry is highly sensitive therefore it is a widely used approach that can separate and identify the small and large biomolecule compounds by their size, mass, shape and charge. IMS is a type of pre-filter for mass spectrometry (Cumeras *et al.*, 2016). During an analysis, the molecules are ionized and sent to the drift tube with an electrospray source. Ions are driven from a gas-filled chamber under the influence using an electric field.

In this project, all analytical analysis were performed with Waters SYNAPT G2-Si HDMS instrument (Waters, Manchester, U.S.). For both DnaK₃₉₂ and DnaK₃₈₈ IMS analyses were performed pH-dependent. Representative charge state distribution spectra of DnaK₃₉₂ and DnaK₃₈₈ were shown at Figure 3.9 and Figure 3.11, respectively. The three-dimensional IMS spectra and the drift time distributions of purified DnaK₃₉₂ protein were demonstrated at Figure 3.10. At the alkaline pH, the most efficient charge of DnaK₃₉₂ has, which is +13, chemical shift behaviour. That chemical shift observed as +14. The three-dimensional IMS spectra and the drift time

distributions of purified DnaK₃₈₈ protein were demonstrated at Figure 3.12. Two conformations were observed for DnaK₃₈₈ at all measured pH states. Other replicates are represented in Appendix E. At the alkaline pH, DnaK₃₈₈ remained own charge. Our complementary approach has showed using IMS the linker binding effect on the ATPase domain by favoring the more closed conformation at alkaline pH. Data acquisition was obtained by the DriftScope software Version 2.9.

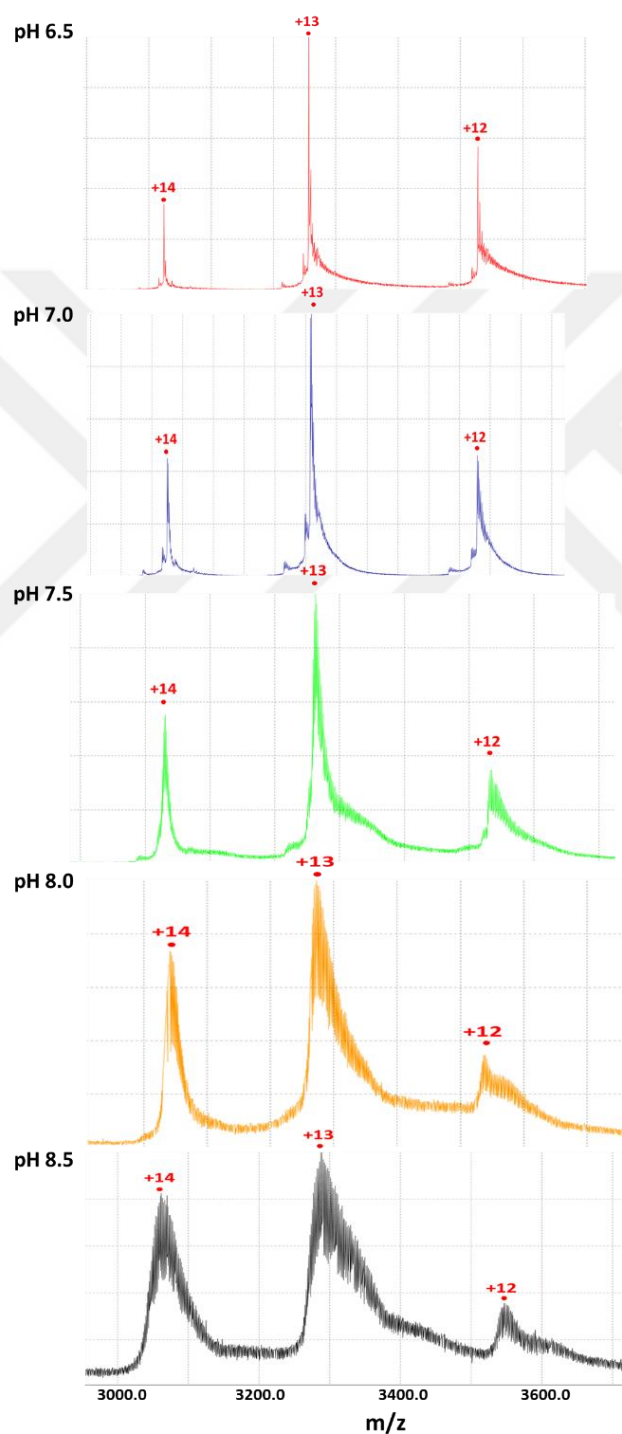


Figure 3.9: Charge state distributions of purified DnaK₃₉₂ protein in a range of pH values.

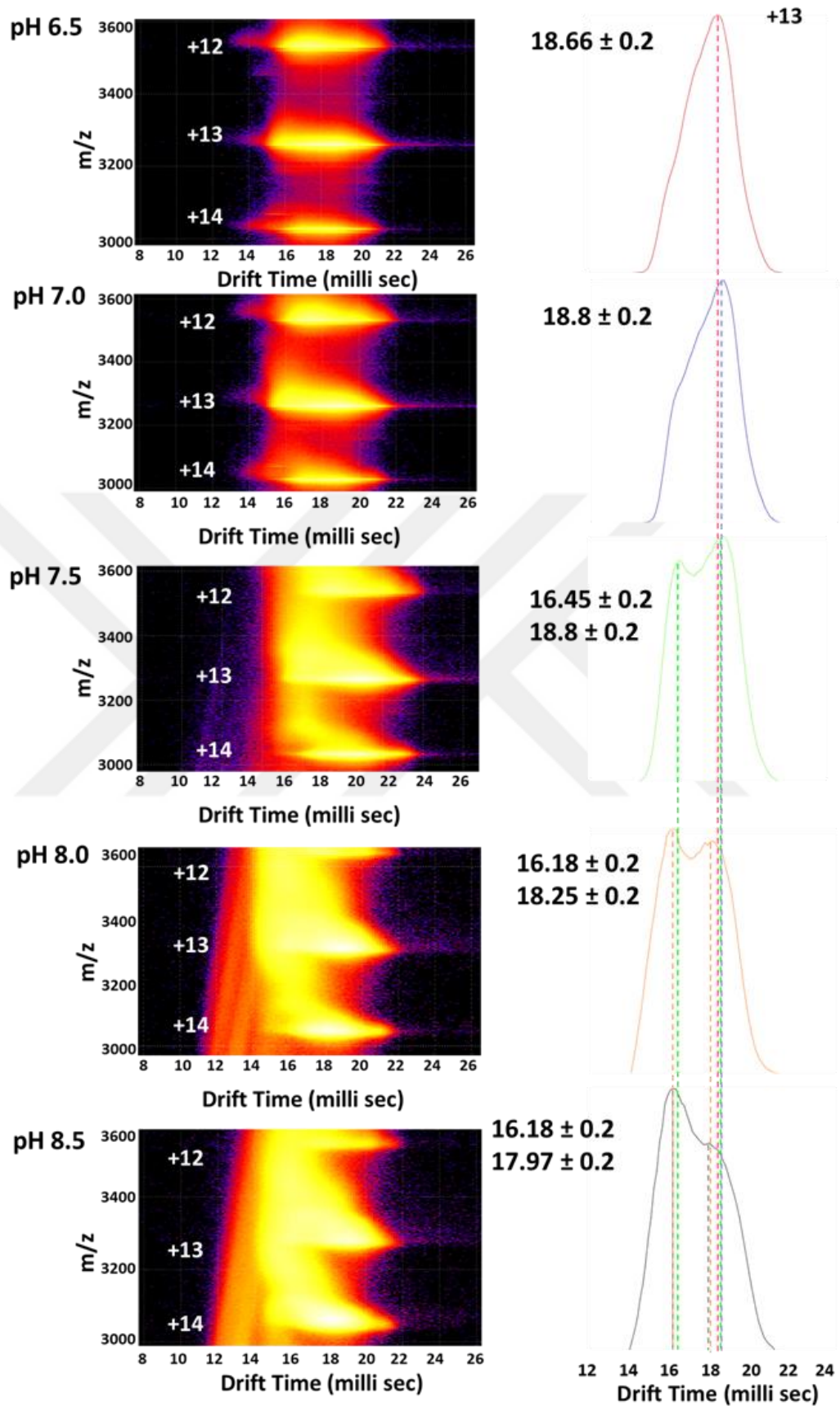


Figure 3.10: IMS analysis of purified DnaK₃₉₂ protein in a range of pH values. The three-dimensional IMS spectra of DnaK₃₉₂ is on the left, and the drift time distribution is on the right.

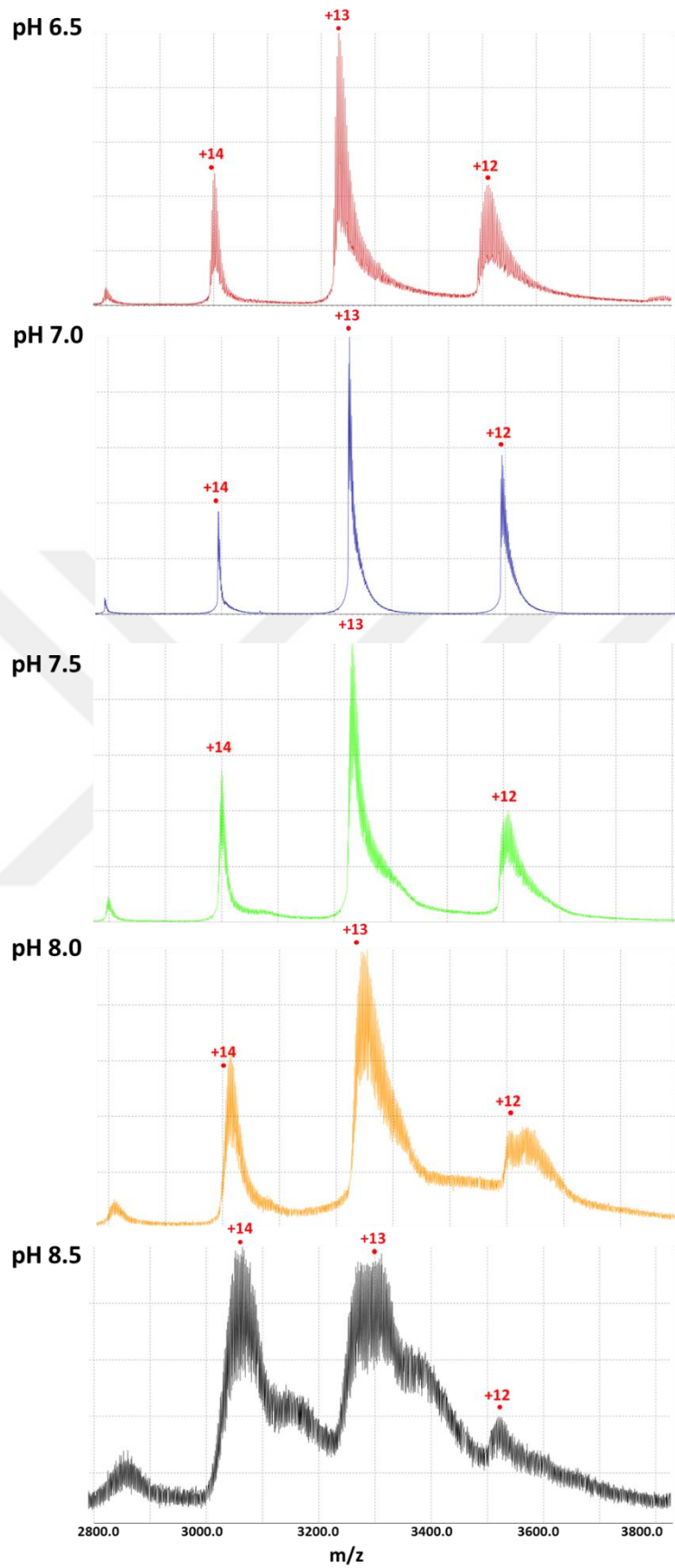


Figure 3.11: Charge state distributions of purified DnaK₃₈₈ protein in a range of pH values

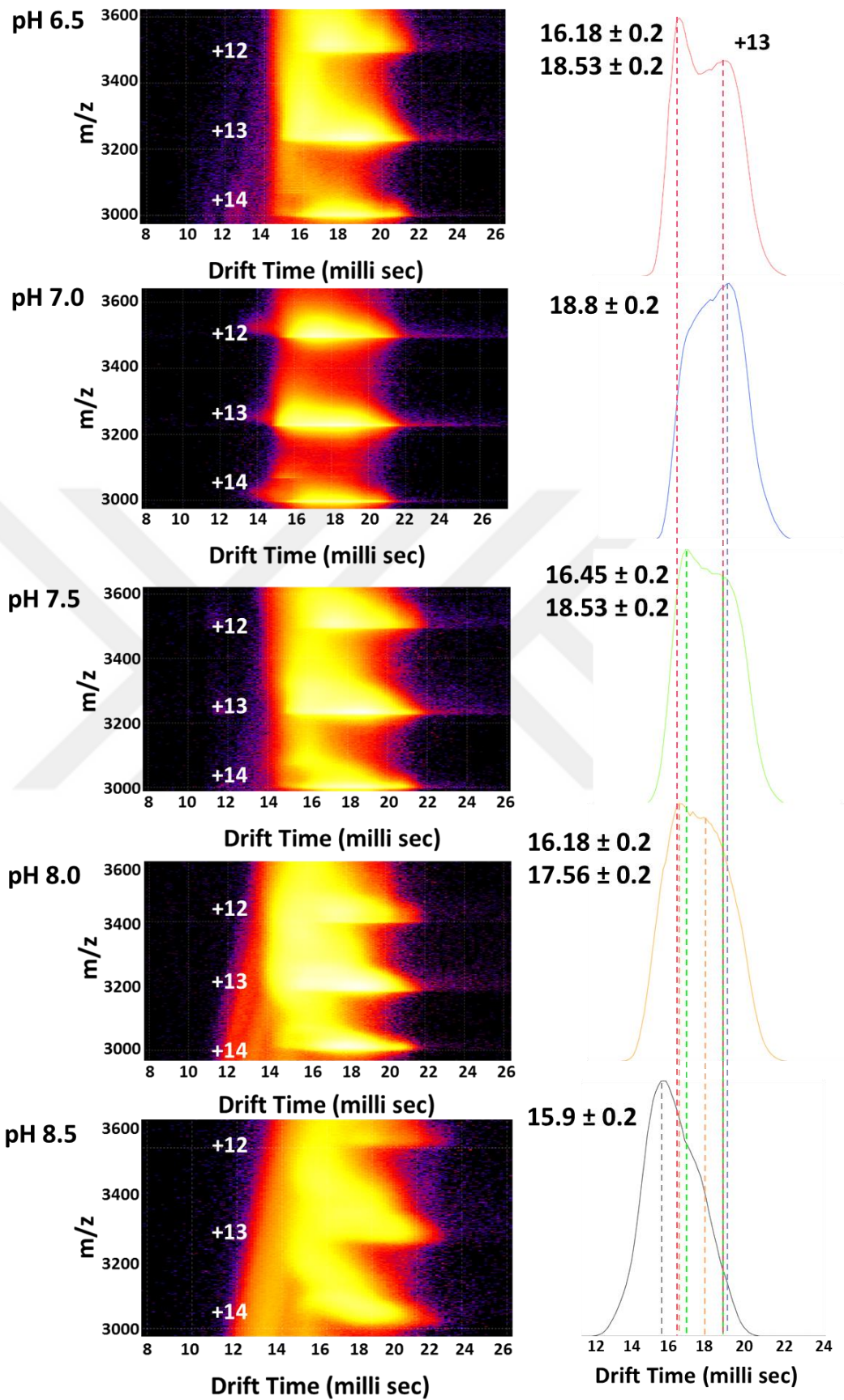


Figure 3.12: IMS analysis of purified DnaK₃₈₈ protein in a range of pH values. The three-dimensional IMS spectra of DnaK₃₈₈ is on the left, and the drift time distribution is on the right.



4. DISCUSSION

Proteins are dynamic entities that settle structural communities, and most of the protein functions depend upon their dynamic character. Hsp70s are structurally landscaped allosteric molecular chaperones, including large rearrangements of the nucleotide binding domain and substrate binding domain in response to adenine nucleotides and substrates. The Hsp70 conformational ensemble is populated at the allosteric cycle and the control of these populations of ligands is unravel yet. The distribution of proteins in equilibrium is difficult to detect in the native state because of the subtle differences. These subtle differences can only be captured with protein dynamic studies instead of conventional methods. This study is a good example for detecting the distribution of proteins in the equilibrium state. In this study, we looked at the linker induced effects in the ATPase domain where different conformational ensembles can be obtained with subtle conformational changes. Similar conformational changes were observed in Lai *et al.*, (2017), Matthias P Mayer and Gierasch, (2018), and Anastasia Zhuravleva *et al.*, (2012) studies.

We analyzed the conformational species that are under different ligand binding conditions during the allosteric cycle of *E. coli* Hsp70 DnaK by two different analyses, ion-mobility mass spectrometry (IM-MS) and native mass spectrometry.

Ion-mobility mass spectrometry was employed to investigate different conformations populated in the purified samples. We were focused on +13 charge states of the DnaK₃₉₂ and DnaK₃₈₈ which is the most intense charge state peak. We were investigated the 3-dimensional conformational distribution in terms of mass, charge and size. Since the distinguishing feature in the pH-dependent assay was an alteration in size, we aimed to observe drift time change due to their size differences. Conformational distributions can be found with analytical IM-MS technique at the equilibrium state. DnaK₃₉₂ has the partial interdomain linker (³⁸⁹VLLL³⁹²) linker, therefore, it has distribution differences by DnaK₃₈₈. With the lead of these finding and our results, below pH 7.5 there is predominantly one population being observed, with the pH increase two distinct conformations of DnaK₃₉₂ were determined by IM-MS as

demonstrated in Figure 3.9. However, two conformations were observed at all measured pH states for DnaK₃₈₈ as shown in Figure 3.10. According to Swain *et al.*, (2007) at alkaline pH linker of DnaK₃₉₂ loses its compactness and functionality and our findings show correlation with their dissertation. In contrast to their claim, we have obtained +13 charge state instead of +14 as the most abundant charge state in DnaK₃₈₈ at pH 7.5.

Interestingly, increasing buffer pH in DnaK₃₉₂ creates another conformational population that shifted lower drift time. In fact that, we can obviously assert that decreased drift time demonstrates newly-formed population has smaller and more compact three-dimensional structure than initial conformation. This could be the outcome of increasing interaction between the linker and Nucleotide Binding Domain (NBD).

Consequently, there are different conformational states associated with the binding of the linker and we have proved it in this study. Lai *et al.*, (2017), Matthias P Mayer and Gierasch, (2018), and Anastasia Zhuravleva *et al.*, (2012) studies support our results. We predict that these ensembles will perform more detailed dynamic simulation studies. For more detailed results of these studies, we can implement mutational screening and then analyze it with native mass spectrometry and IM-MS studies. Additionally, *in-silico* studies must be done for more details. Thus, the ensemble distribution of proteins can be determined.

REFERENCES

- Alderson, T. R. R., Kim, J. H. H., & Markley, J. L. L.** (2016). Dynamical Structures of Hsp70 and Hsp70-Hsp40 Complexes. *Structure*, 24(7), 1014–1030. <https://doi.org/10.1016/j.str.2016.05.011>
- Azem, A., Oppliger, W., Lustig, A., Jenö, P., Feifel, B., Schatz, G., & Horst, M.** (1997). The Mitochondrial hsp70 chaperone system. *Biochemistry*, 272(33), 20901–20906. <https://doi.org/10.1074/jbc.272.33.20901>
- Bascos, N. A. D., Mayer, M. P., Bukau, B., & Landry, S. J.** (2017). The Hsp40 J-domain modulates Hsp70 conformation and ATPase activity with a semi-elliptical spring. *Protein Science*, 26(9), 1838–1851. <https://doi.org/10.1002/pro.3223>
- Ben-Nissan, G., & Sharon, M.** (2018). The application of ion-mobility mass spectrometry for structure/function investigation of protein complexes. *Current Opinion in Chemical Biology*, 42, 25–33. <https://doi.org/10.1016/j.cbpa.2017.10.026>
- Bertelsen, E. B., Chang, L., Gestwicki, J. E., & Zuiderweg, E. R. P.** (2009). Solution conformation of wild-type E. coli Hsp70 (DnaK) chaperone complexed with ADP and substrate. *Proceedings of the National Academy of Sciences*. <https://doi.org/10.1073/pnas.0903503106>
- Borges, T. J., Wieten, L., Van Herwijnen, M. J. C., Broere, F., Van der Zee, R., Bonorino, C., & Van Eden, W.** (2012). The anti-inflammatory mechanisms of Hsp70. *Frontiers in Immunology*. <https://doi.org/10.3389/fimmu.2012.00095>
- Brehme, M., & Voisine, C.** (2016). Model systems of protein-misfolding diseases reveal chaperone modifiers of proteotoxicity. *Disease Models & Mechanisms*, 9(8), 823–838. <https://doi.org/10.1242/dmm.024703>
- Bukau, B., & Horwich, A. L.** (1998). The Hsp70 and Hsp60 chaperone machines. *Cell*. [https://doi.org/10.1016/S0092-8674\(00\)80928-9](https://doi.org/10.1016/S0092-8674(00)80928-9)
- Chang, L., Thompson, A. D., Ung, P., Carlson, H. A., & Gestwicki, J. E.** (2010). Mutagenesis reveals the complex relationships between ATPase rate and the chaperone activities of Escherichia coli heat shock protein 70 (Hsp70/DnaK). *Journal of Biological Chemistry*, 285(28), 21282–21291. <https://doi.org/10.1074/jbc.M110.124149>
- Chiappori, F., Merelli, I., Colombo, G., Milanesi, L., & Morra, G.** (2012). Molecular Mechanism of Allosteric Communication in Hsp70 Revealed by Molecular Dynamics Simulations. *PLoS Computational Biology*, 8(12). <https://doi.org/10.1371/journal.pcbi.1002844>
- Corrêa, D. H. A., & Ramos, C. H. I.** (2009). The use of circular dichroism spectroscopy to study protein folding, form and function. *African J. Biochem. Res.*, 3(June 2014), 164–173. <https://doi.org/not available>
- Cumeras, R., Figueras, E., Davis, C. E., Baumbach, J. I., & Chemistry, A.** (2016). HHS Public Access, 140(5), 1376–1390. <https://doi.org/10.1039/c4an01100g.Review>
- Dou, F., Netzer, W. J., Tanemura, K., Li, F., Hartl, F. U., Takashima, A., ... Xu,**

- H.** (2003). Chaperones increase association of tau protein with microtubules. *Proceedings of the National Academy of Sciences of the United States of America*, *100*(2), 721–726. <https://doi.org/10.1073/pnas.242720499>
- Esser, C., Alberti, S., & Höhfeld, J.** (2004). Cooperation of molecular chaperones with the ubiquitin/proteasome system. *Biochimica et Biophysica Acta - Molecular Cell Research*. <https://doi.org/10.1016/j.bbamcr.2004.09.020>
- Ewing, R. G., Atkinson, D. A., Eiceman, G. A., & Ewing, G. J.** (2001). 1-s2.0-S0039914000005658-main, *54*, 1–15. [https://doi.org/10.1016/S0039-9140\(00\)00565-8](https://doi.org/10.1016/S0039-9140(00)00565-8)
- Fan, C. Y., Lee, S., & Cyr, D. M.** (2003). Mechanisms for regulation of Hsp70 function by Hsp40. *Cell Stress and Chaperones*. [https://doi.org/10.1379/1466-1268\(2003\)008<0309:MFROHF>2.0.CO;2](https://doi.org/10.1379/1466-1268(2003)008<0309:MFROHF>2.0.CO;2)
- Feder, M. E., & Hofmann, G. E.** (1999). Heat-shock proteins, molecular chaperones, and the stress response: evolutionary and ecological physiology. *Annual Review of Physiology*, *61*, 243–282. <https://doi.org/10.1146/annurev.physiol.61.1.243>
- Gober, M. D., Wales, S. Q., & Aurelian, L.** (2005). Herpes simplex virus type 2 encodes a heat shock protein homologue with apoptosis regulatory functions. *Frontiers in Bioscience*, *10*, 2788–2803.
- Hartl, F. U., & Hayer-Hartl, M.** (2002). Protein folding. Molecular chaperones in the cytosol: From nascent chain to folded protein. *Science*. <https://doi.org/10.1126/science.1068408>
- Hendrick, J. P., & Hartl, F.-U.** (1993). Molecular Chaperone Functions of Heat-Shock Proteins. *Annual Review of Biochemistry*, *62*(1), 349–384. <https://doi.org/10.1146/annurev.bi.62.070193.002025>
- Hipp, M. S., Park, S. H., & Hartl, U. U.** (2014). Proteostasis impairment in protein-misfolding and -aggregation diseases. *Trends in Cell Biology*. <https://doi.org/10.1016/j.tcb.2014.05.003>
- Jäättelä, M., Wissing, D., Kokholm, K., Kallunki, T., & Egeblad, M.** (1998). Hsp70 exerts its anti-apoptotic function downstream of caspase-3-like proteases. *EMBO Journal*, *17*(21), 6124–6134. <https://doi.org/10.1093/emboj/17.21.6124>
- Jiang, J., Lafer, E. M., & Sousa, R.** (2006). Crystallization of a functionally intact Hsc70 chaperone. *Acta Crystallographica Section F: Structural Biology and Crystallization Communications*. <https://doi.org/10.1107/S1744309105040303>
- Kityk, R., Kopp, J., Sinning, I., & Mayer, M. P.** (2012). Structure and Dynamics of the ATP-Bound Open Conformation of Hsp70 Chaperones. *Molecular Cell*, *48*(6), 863–874. <https://doi.org/10.1016/j.molcel.2012.09.023>
- Kityk, R., Vogel, M., Schlecht, R., Bukau, B., & Mayer, M. P.** (2015). Pathways of allosteric regulation in Hsp70 chaperones. *Nature Communications*, *6*, 1–11. <https://doi.org/10.1038/ncomms9308>
- Knapman, T. W., Valette, N. M., Warriner, S. L., & Ashcroft, A. E.** (2013). Ion Mobility Spectrometry-Mass Spectrometry of Intrinsically Unfolded Proteins: Trying to Put Order into Disorder. *Current Analytical Chemistry*, *9*(0), 181–191. <https://doi.org/10.2174/1573411011309020004>
- Labrador-garrido, A., Bertocini, C. W., & Roodveldt, C.** (2010). The Hsp70 Chaperone System in Parkinson's Disease. *Regenerative Medicine*, (May 2014). <https://doi.org/10.5772/16671>
- Lai, A. L., Clerico, E. M., Blackburn, M. E., Patel, N. A., Robinson, C. V., Borbat, P. P., ... Gierasch, L. M.** (2017). Key features of an Hsp70 chaperone allosteric landscape revealed by ion-mobility native mass spectrometry and double electron-electron resonance. *Journal of Biological Chemistry*, *292*(21), 8773–

8785. <https://doi.org/10.1074/jbc.M116.770404>

- Lanucara, F., Holman, S. W., Gray, C. J., & Evers, C. E.** (2014). The power of ion mobility-mass spectrometry for structural characterization and the study of conformational dynamics. *Nature Chemistry*, 6(4), 281–294. <https://doi.org/10.1038/nchem.1889>
- Leney, A. C., & Heck, A. J. R.** (2017). Native Mass Spectrometry: What is in the Name? *Journal of the American Society for Mass Spectrometry*, 28(1), 5–13. <https://doi.org/10.1007/s13361-016-1545-3>
- Liang, P., & MacRae, T. H.** (1997). Molecular chaperones and the cytoskeleton. *Journal of Cell Science*, 110 (Pt 1(13), 1431–1440. Retrieved from <http://jcs.biologists.org/content/110/13/1431.abstract>
- Makhnevych, T., & Houry, W. A.** (2012). The role of Hsp90 in protein complex assembly. *Biochimica et Biophysica Acta - Molecular Cell Research*. <https://doi.org/10.1016/j.bbamcr.2011.09.001>
- Malinverni, D., Lopez, A. J., De Los Rios, P., Hummer, G., & Barducci, A.** (2017). Modeling Hsp70/Hsp40 interaction by multi-scale molecular simulations and coevolutionary sequence analysis. *ELife*, 6, 1–20. <https://doi.org/10.7554/eLife.23471>
- Mayer, M. P.** (2013). Hsp70 chaperone dynamics and molecular mechanism. *Trends in Biochemical Sciences*. <https://doi.org/10.1016/j.tibs.2013.08.001>
- Mayer, M. P., & Bukau, B.** (2005). Hsp70 chaperones: Cellular functions and molecular mechanism. *Cellular and Molecular Life Sciences*, 62(6), 670–684. <https://doi.org/10.1007/s00018-004-4464-6>
- Mayer, M. P., & Gierasch, L. M.** (2018). Recent advances in the structural and mechanistic aspects of Hsp70 molecular chaperones. *Journal of Biological Chemistry*, (November), jbc.REV118.002810. <https://doi.org/10.1074/jbc.REV118.002810>
- Mori, K., Kawahara, T., Yoshida, H., Yanagi, H., & Yura, T.** (1996). Signalling from endoplasmic reticulum to nucleus: transcription factor with a basic-leucine zipper motif is required for the unfolded protein-response pathway. *Genes to Cells*, 1(9), 803–817. <https://doi.org/10.1046/j.1365-2443.1996.d01-274.x>
- Pratt, W. B., Morishima, Y., Peng, H. M., & Osawa, Y.** (2010). Proposal for a role of the Hsp90/Hsp70-based chaperone machinery in making triage decisions when proteins undergo oxidative and toxic damage. *Experimental Biology and Medicine*. <https://doi.org/10.1258/ebm.2009.009250>
- Qi, R., Sarbeng, E. B., Liu, Q., Le, K. Q., Xu, X., Xu, H., ... Liu, Q.** (2013). Allosteric opening of the polypeptide-binding site when an Hsp70 binds ATP. *Nature Structural and Molecular Biology*, 20(7), 900–907. <https://doi.org/10.1038/nsmb.2583>
- Ratheesh Kumar, R., Nagarajan, N. S., Arunraj, S. P., Sinha, D., Veedin Rajan, V. B., Esthaki, V. K., & D'Silva, P.** (2012). HSPiR: A manually annotated heat shock protein information resource. *Bioinformatics*. <https://doi.org/10.1093/bioinformatics/bts520>
- Ritossa, F.** (1962). A new puffing pattern induced by temperature shock and DNP in drosophila. *Experientia*, 18(12), 571–573. <https://doi.org/10.1007/BF02172188>
- Rodriguez, F., Arsène-Plöetze, F., Rist, W., Rüdiger, S., Schneider-Mergener, J., Mayer, M. P., & Bukau, B.** (2008). Molecular Basis for Regulation of the Heat Shock Transcription Factor σ 32 by the DnaK and DnaJ Chaperones. *Molecular Cell*, 32(3), 347–358. <https://doi.org/10.1016/j.molcel.2008.09.016>
- Rüdiger, S., Germeroth, L., Schneider-Mergener, J., & Bukau, B.** (1997).

- Substrate specificity of the DnaK chaperone determined by screening cellulose-bound peptide libraries. *EMBO Journal*, 16(7), 1501–1507. <https://doi.org/10.1093/emboj/16.7.1501>
- Sambrook, J., & Russell, D. W.** (2006). The Inoue Method for Preparation and Transformation of Competent *E. Coli*: “Ultra-Competent” Cells. *Cold Spring Harbor Protocols*, 2006(1), pdb.prot3944. <https://doi.org/10.1101/pdb.prot3944>
- Swain, J. F., Dinler, G., Sivendran, R., Montgomery, D. L., Stotz, M., & Gierasch, L. M.** (2007). Hsp70 Chaperone Ligands Control Domain Association via an Allosteric Mechanism Mediated by the Interdomain Linker. *Molecular Cell*, 26(1), 27–39. <https://doi.org/10.1016/j.molcel.2007.02.020>
- Swain, J. F., Schulz, E. G., & Gierasch, L. M.** (2006). Direct comparison of a stable isolated Hsp70 substrate-binding domain in the empty and substrate-bound states. *Journal of Biological Chemistry*, 281(3), 1605–1611. <https://doi.org/10.1074/jbc.M509356200>
- Uchida, T., & Kanemori, M.** (2018). Two J domains ensure high cochaperone activity of DnaJ, Escherichia coli heat shock protein 40. *Journal of Biochemistry*, 164(2), 153–163. <https://doi.org/10.1093/jb/mvy038>
- Ung, P. M. U., Thompson, A. D., Chang, L., Gestwicki, J. E., & Carlson, H. A.** (2013). Identification of Key Hinge Residues Important for Nucleotide-Dependent Allostery in *E. coli* Hsp70/DnaK. *PLoS Computational Biology*, 9(11), 1–11. <https://doi.org/10.1371/journal.pcbi.1003279>
- Wei, Y., Thyparambil, A. A., & Latour, R. A.** (2016). HHS Public Access, 1844(12), 2331–2337. <https://doi.org/10.1016/j.bbapap.2014.10.001>.Protein
- Young, J. C.** (2010). Mechanisms of the Hsp70 chaperone system. *Biochemistry and Cell Biology*, 88(2), 291–300. <https://doi.org/10.1139/o09-175>
- Young, J. C., Barral, J. M., & Hartl, F. U.** (2003). More than folding: Localized functions of cytosolic chaperones. *Trends in Biochemical Sciences*. <https://doi.org/10.1016/j.tibs.2003.08.009>
- Zheng, X., Wojcik, R., Zhang, X., Ibrahim, Y. M., Burnum-Johnson, K. E., Orton, D. J., ... Baker, E. S.** (2017). Coupling Front-End Separations, Ion Mobility Spectrometry, and Mass Spectrometry For Enhanced Multidimensional Biological and Environmental Analyses. *Annual Review of Analytical Chemistry*. <https://doi.org/10.1146/annurev-anchem-061516-045212>
- Zhu, X., Zhao, X., Burkholder, W. F., Gragerov, A., Ogata, C. M., Gottesman, M. E., & Hendrickson, W. A.** (1996). Structural Analysis of Substrate Binding by the Molecular Chaperone DnaK. *Science*, 272(5268), 1606–1614. <https://doi.org/10.1126/science.272.5268.1606>
- Zhuravleva, A., Clerico, E. M., & Gierasch, L. M.** (2012). An interdomain energetic tug-of-war creates the allosterically active state in Hsp70 molecular chaperones. *Cell*. <https://doi.org/10.1016/j.cell.2012.11.002>
- Zhuravleva, A., & Gierasch, L. M.** (2011). Allosteric signal transmission in the nucleotide-binding domain of 70-kDa heat shock protein (Hsp70) molecular chaperones. *Proceedings of the National Academy of Sciences*, 108(17), 6987–6992. <https://doi.org/10.1073/pnas.1014448108>

APPENDICES

APPENDIX A: Laboratory Equipments

APPENDIX B: Chemicals and Enzymes

APPENDIX C: Buffers and Solutions

APPENDIX D: Results of the Sequencing Data of DnaK in *E. coli*

APPENDIX E: Replicates of the Results



APPENDIX A

Table A.1: Laboratory equipments used in the experiments.

Equipment	Company
Autoclave	Zealway GR110DF
Balance	Precisa BJ 610C
Centrifuges	VWR Mega Star 3.0R
Circular Dichroism	Jasco J-1500
Deep Freezer	-80°C Aucma
Electrophoresis Gel System	Cleaver Scientific
FPLC	ÄKTA Avant 25, ÄKTA Start
FPLC Columns	GE Healthcare, Biorad Econo- Column
Freezers	Bosch -20°C
Gel Screening System	BioRad ChemiDoc™ MP BioRad Gel Doc™ XR+
Heat Block	BioSan Bio TDB-100
Ice Machine	Scotsman AF 80
Laminar Air Flow Cabinets	FASTER BH-EN 2003
Magnetic Stirrer	Dragon Lab, MS-H-S
Mass Spectrometry	Waters Synapt G2-Si
Micropipettes	Thermo Scientific
Microplate Spectrophotometer	BMG LABTECH CLARIOstar®
Mini centrifuge	Inovia Technology MINO-10K
Orbital Shaker	Lab Companion™ ISF-7200
pH Meter	Mettler Toledo
Power Supply	GE Healthcare
Precision Balance	Precisa XB 220A

Table A.1: Laboratory equipments used in the experiments (continued).

Equipment	Company
Pure Water System	Merck Direct-Q [®]
Shaker	Heidolph Duomax 1030
SDS-PAGE Gel Electrophoresis System	Biorad
Ultracentrifuges	HITACHI CR 22N ScanSpeed 1730R
Ultrapure Water System	Merck Direct-Q [®] 3UV
Ultrasonic Bath	Bandelin Sonorex
UV-Visible Spectrophotometer	Shimadzu UV-1700 Thermo Scientific Nanodrop 2000
Vortex	Dragon Lab MX-F
Water Bath	Memmert WB110

APPENDIX B

Table B.1: Chemicals and Enzymes used in the experiments.

Chemicals and Enzymes	Company
40 % Acrylamide Solution	Biorad
Acetic acid	Sigma-Aldrich
Agar Bacteriological Grade	Multicell
Agarose	Multicell
Ampicillin	Roth
APS	Sigma
ATP	Sigma
ATP agarose	Sigma
Bromophenol Blue	Sigma-Aldrich
Calcium chloride	Merck
Chloramphenicol	AppliChem
Coomassie brilliant blue	Sigma-Aldrich
DMSO	Biomatik
DNase I	BioLabs
EDTA	Molecula
Ethanol	Merck
Glycerol	Multicell
Hepes	Multicell
HiTrap DEAE Sepharose column	GE Healthcare
Hydrochloric Acid	Sigma-Aldrich
IPTG	Sigma
Laemmli protein sample buffer	Sigma
Leupeptin	Roth

Table B.1: Chemicals and Enzymes used in the experiments (continued).

Chemicals and Enzymes	Company
Lysosyme	Roth
Magnesium Acetate	Merck
Magnesium Chloride	Merck
Manganese (II) Chloride	Sigma-Aldrich
PageRuler Prestained Protein Ladder	Thermo Scientific
PEP	Sigma
Peptone from casein pancreatically digested	Merck
Phosphoenol pyruvate	Aldrich
PIPES	PanReac AppliChem
PK/LDH	Sigma
PMSF	Fluka
Potassium Chloride	Carlo Erba Reagents
Protease cocktail inhibitor	Roche
Pyruvate kinase	Sigma
SDS	Bioshop
Sodium Chloride	Merck
Sodium Hydroxide	ChemCruz
SYBR Green	Roche
Tris	Multicell
Yeast Extract	Sigma-Aldrich
β -mercaptoethanol	Sigma
β -NADH	Sigma

APPENDIX C

Luria Bertani (LB) medium: It was prepared for bacterial growth. 10 g tryptone, 5 g yeast extract, and 10 g NaCl was dissolved in 1 L dH₂O. After dissolving, media was sterilized by autoclaving at 121°C for 15 minutes. When medium was getting cooled, for making selection, appropriate antibiotics (ampicillin - chloramphenicol) were added.

Luria Bertani (LB) agar: It was prepared for bacterial growth in plate. 10 g tryptone, 5 g yeast extract, 20g agar and 10 g NaCl was dissolved in 1 L dH₂O. After dissolving, media was sterilized by autoclaving at 121°C for 15 minutes. When medium was getting cooled, for making selection, appropriate antibiotics (ampicillin - chloramphenicol) were added, and LB agar was poured in plates.

Resuspension buffer: It was used for dissolving BB1553 cells in the growth step. 20 mM Tris, 50 mM NaCl, 0.1 mM EDTA were dissolved in 1 L dH₂O. pH was adjusted to 7.4. Then, it was filtered by 0.2 µm pore filter for sterilization.

Starting buffer: It was used in the DnaK Anion Purification by HiTrap DEAE Sepharose FF. 20 mM Tris-HCl, 1 mM EDTA were dissolved in 1 L ddH₂O. pH was adjusted to 7.4. Then, it was filtered by 0.2 µm pore filter for sterilization.

Elution buffer: It was used in the DnaK Anion Purification by HiTrap DEAE Sepharose FF. 20 mM Tris-HCl, 1 mM EDTA and 1 M NaCl were dissolved in 1 L ddH₂O. pH was adjusted to 7.4. Then, it was filtered by 0.2 µm pore filter for sterilization.

HMK (Binding) buffer: It was used in the DnaK Affinity Purification by ATP-agarose column. 20 mM HEPES, 5 mM MgCl₂ and 100 mM KCl were dissolved in 1 L ddH₂O. pH was adjusted to 7.4. Then, it was filtered by 0.2 µm pore filter for sterilization.

HEK (Elution) buffer: It was used in the DnaK Affinity Purification by ATP-agarose column. 20 mM HEPES, 2 mM EDTA and 100 mM KCl were dissolved in 1 L ddH₂O. pH was adjusted to 7.4. Then, it was filtered by 0.2 µm pore filter for sterilization.

Washing buffer 1: It was used in the DnaK Affinity Purification by ATP-agarose column. 10 mM EDTA and 100 mM KCl were dissolved in 1 L ddH₂O. pH was adjusted to 7.4. Then, it was filtered by 0.2 µm pore filter for sterilization.

Washing buffer 2: It was used in the DnaK Affinity Purification by ATP-agarose column. HMK buffer and 2 M KCl were dissolved in 1 L ddH₂O. pH was adjusted to 7.4. Then, it was filtered by 0.2 µm pore filter for sterilization.

Running buffer (10X): It was used in SDS-PAGE analysis during the running process. 30.3 g Tris, 144 g glycine and 10 g SDS were dissolved in 1L with dH₂O. 10X Running buffer was diluting to 1X Running buffer with dH₂O.

Coomassie Brilliant Blue stain solution: It was used during staining SDS-PAGE gels. 1 g Coomassie brilliant blue R-250 was mixed with 400 mL methanol, 100 mL acetic acid and dH₂O was added up to 1 mL.

Destain solution: It was used during destaining SDS-PAGE gels. 400 mL methanol, 100 mL acetic acid and dH₂O was added up to 1 mL.



APPENDIX D

DnaK ₃₉₂	15	TTTCGAT-TTCTATTATCG-AATCGACGAAGTTGACGGCGAAAAACCTTCGAAGTTCT	72
wtDnaK	597	TTTCGATATTTCTATTATCGAAATCGACGAAGTTGACGGCGAAAAACCTTCGAAGTTCT	656
DnaK ₃₉₂	73	GGCAACCAACGGTGATACCCACCTGGGGGGTGAAGACTTCGACAGCCGTCTGATCAACTA	132
wtDnaK	657	GGCAACCAACGGTGATACCCACCTGGGGGGTGAAGACTTCGACAGCCGTCTGATCAACTA	716
DnaK ₃₉₂	133	TCTGGTTGAAGAATTCAGAAAGATCAGGGCATTGACCTGCGCAACGATCCGCTGGCAAT	192
wtDnaK	717	TCTGGTTGAAGAATTCAGAAAGATCAGGGCATTGACCTGCGCAACGATCCGCTGGCAAT	776
DnaK ₃₉₂	193	GCAGCGCCTGAAAGAAGCGGCAGAAAAAGCGAAAATCGAACTGTCTTCCGCTCAGCAGAC	252
wtDnaK	777	GCAGCGCCTGAAAGAAGCGGCAGAAAAAGCGAAAATCGAACTGTCTTCCGCTCAGCAGAC	836
DnaK ₃₉₂	253	CGACGTTAACCTGCCATACATCACTGCAGACGCGACCGGTCCGAAACACATGAACATCAA	312
wtDnaK	837	CGACGTTAACCTGCCATACATCACTGCAGACGCGACCGGTCCGAAACACATGAACATCAA	896
DnaK ₃₉₂	313	AGTGACTCGTGCGAAACTGGAAAGCCTGGTTGAAGATCTGGTAAACCGTTCATTGAGCC	372
wtDnaK	897	AGTGACTCGTGCGAAACTGGAAAGCCTGGTTGAAGATCTGGTAAACCGTTCATTGAGCC	956
DnaK ₃₉₂	373	GCTGAAAGTTGCACTGCAGGACGCTGGCCTGTCCGTATCTGATATCGACGACGTTATCCT	432
wtDnaK	957	GCTGAAAGTTGCACTGCAGGACGCTGGCCTGTCCGTATCTGATATCGACGACGTTATCCT	1016
DnaK ₃₉₂	433	CGTTGGTGGTCAGACTCGTATGCCAATGGTTCAGAAGAAAGTTGCTGAGTTCTTTGGTAA	492
wtDnaK	1017	CGTTGGTGGTCAGACTCGTATGCCAATGGTTCAGAAGAAAGTTGCTGAGTTCTTTGGTAA	1076
DnaK ₃₉₂	493	AGAGCCGCGTAAAGACGTTAACCCGGACGAAGCTGTAGCAATCGGTGCTGCTGTTTCAGGG	552
wtDnaK	1077	AGAGCCGCGTAAAGACGTTAACCCGGACGAAGCTGTAGCAATCGGTGCTGCTGTTTCAGGG	1136
DnaK ₃₉₂	553	TGGTGTTCGACTGGTGACGTAAGACGTAAGACTGCTGCTGCTG	592
wtDnaK	1137	TGGTGTTCGACTGGTGACGTAAGACGTAAGACTGCTGCTGCTG	1176

Figure D.1: The alignment of sequence data of DnaK₃₉₂

DnaK ₃₈₈	15	GCGCTGCATTGCCAGCGGATCGTTGCGCAGGTCAATGCCCTGATCTTTCTTGAATTC TTC	74
WtDnaK	783	 GCGCTGCATTGCCAGCGGATCGTTGCGCAGGTCAATGCCCTGATCTTTCTTGAATTC TTC	724
DnaK ₃₈₈	75	AACCAGATAGTTGATCAGACGGCTGTCGAAGTCTTCACCCCCAGGTGGGTATCACCGTT	134
WtDnaK	723	 AACCAGATAGTTGATCAGACGGCTGTCGAAGTCTTCACCCCCAGGTGGGTATCACCGTT	664
DnaK ₃₈₈	135	GGTTGCCAGAACTTCGAAGGTTTTTCGCGCTCAACTTCGTCGATTTTCGATAATAGAAAT	194
WtDnaK	663	 GGTTGCCAGAACTTCGAAGGTTTTTCGCGCTCAACTTCGTCGATTTTCGATAATAGAAAT	604
DnaK ₃₈₈	195	ATCGAAAGTACCACCACCAGGTCATAAACCCGCGATAGTACGGTTGCCAGTGCCTTTGTC	254
WtDnaK	603	 ATCGAAAGTACCACCACCAGGTCATAAACCCGCGATAGTACGGTTGCCAGTGCCTTTGTC	544
DnaK ₃₈₈	255	CAGACCCTAAGCCAGCGCAGCTGCGGTTCGTTGATGATACGTTTTACTTCCAGACC	314
WtDnaK	543	 CAGACCCTAAGCCAGCGCAGCTGCGGTTCGTTGATGATACGTTTTACTTCCAGACC	484
DnaK ₃₈₈	315	AGCGATACGGCTGCGTCTTTGGTTGCCTGACGCTGAGCATCGTTAAAGTATGCCGGTAC	374
WtDnaK	483	 AGCGATACGGCTGCGTCTTTGGTTGCCTGACGCTGAGCATCGTTAAAGTATGCCGGTAC	424
DnaK ₃₈₈	375	GGTGATAACAGCTTCAGTTACCGGTTACCCAGGTAATCTTCAGCGTTTTCTTCat ttt	434
WtDnaK	423	 GGTGATAACAGCTTCAGTTACCGGTTACCCAGGTAATCTTCAGCGTTTTCTTCATTTT	364
DnaK ₃₈₈	435	tttCAGCACTTCAGCAGAAATCTGCGGGCGTGCCATTTCTGGCCTTTAACTTCGACCCA	494
WtDnaK	363	 TTTCAGCACTTCAGCAGAAATCTGCGGGCGTGCCATTTCTGGCCTTTAACTTCGACCCA	304
DnaK ₃₈₈	495	TGCGTCGCCGTTATCAGCAGCAATAATTTTGAACGGCATGATGGAAACATCACGCTGTAC	554
WtDnaK	303	 TGCGTCGCCGTTATCAGCAGCAATAATTTTGAACGGCATGATGGAAACATCACGCTGTAC	244
DnaK ₃₈₈	555	TTCTTCGTCCTGGAAGCGGCGACCAATCAGGCGTTTAATCGCAAACAGAGTGT TTTGCGG	614
WtDnaK	243	 TTCTTCGTCCTGGAAGCGGCGACCAATCAGGCGTTTAATCGCAAACAGAGTGT TTTGCGG	184
DnaK ₃₈₈	615	GTTTCGTCACCTGACGTTTAGCCGGCTGACCAACTAGAGTTTCACCATCCTGGGTATA	674
WtDnaK	183	 GTTTCGTCACCTGACGTTTAGCCGGCTGACCAACTAGAGTTTCACCATCCTGGGTATA	124
DnaK ₃₈₈	675	GGCAATGATAGAAGGCGTGGTGGCATCGCCTTCGGCGTTCTCCAGCACGCGAGGAGTGGT	734
WtDnaK	123	 GGCAATGATAGAAGGCGTGGTGGCATCGCCTTCGGCGTTCTCCAGCACGCGAGGAGTGGT	64
DnaK ₃₈₈	735	GCCATCCATAATCGCTACACAAGAGTTGGTAGTACCCAGGTCGATACCAATTATTTTACC	794
WtDnaK	63	 GCCATCCATAATCGCTACACAAGAGTTGGTAGTACCCAGGTCGATACCAATTATTTTACC	4
DnaK ₃₈₈	795	CAT 797	
WtDnaK	3	 CAT 1	

Figure D. 2: The alignment of sequence data of DnaK₃₈₈

APPENDIX E

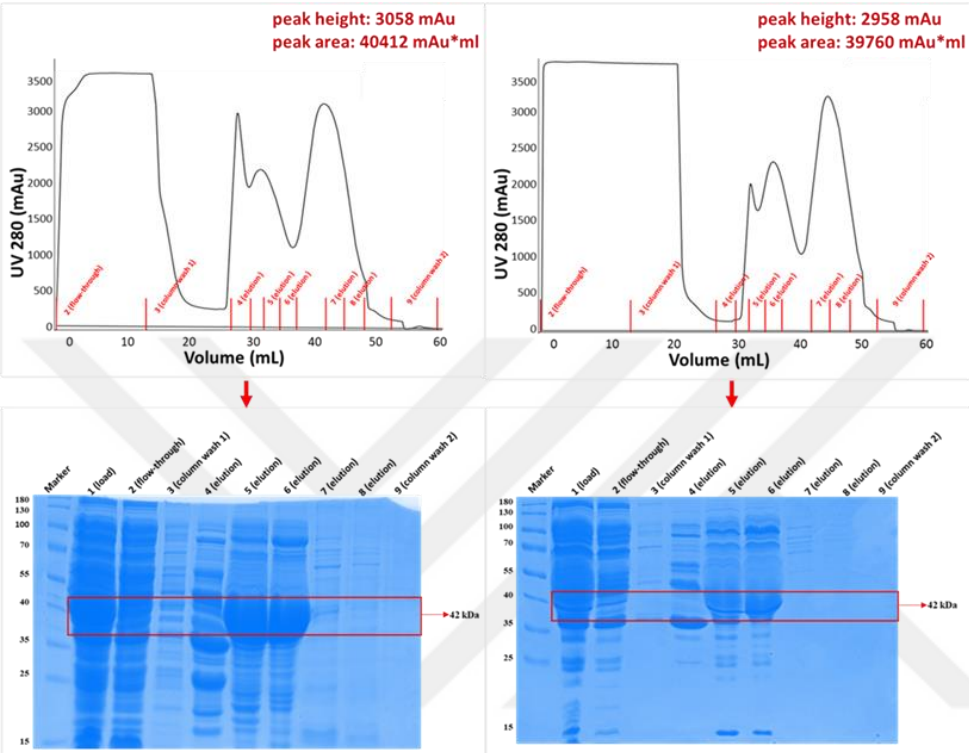


Figure E.1: Replicates of Anion Exchange Chromatograms of DnaK392 (above) and Anion exchange chromatography fractions of DnaK392 by SDS-PAGE (below).

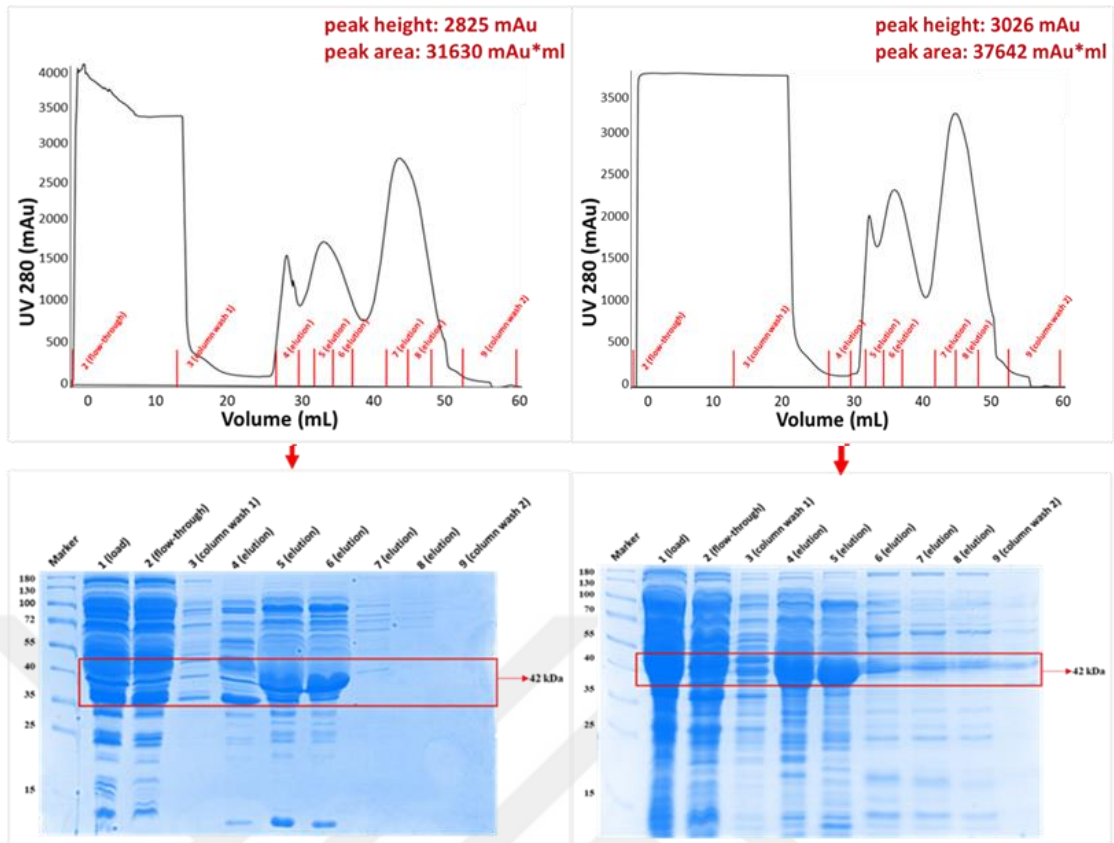


Figure E.2: Replicates of Anion Exchange Chromatograms of DnaK388 (above) and Anion exchange chromatography fractions of DnaK388 by SDS-PAGE (below).

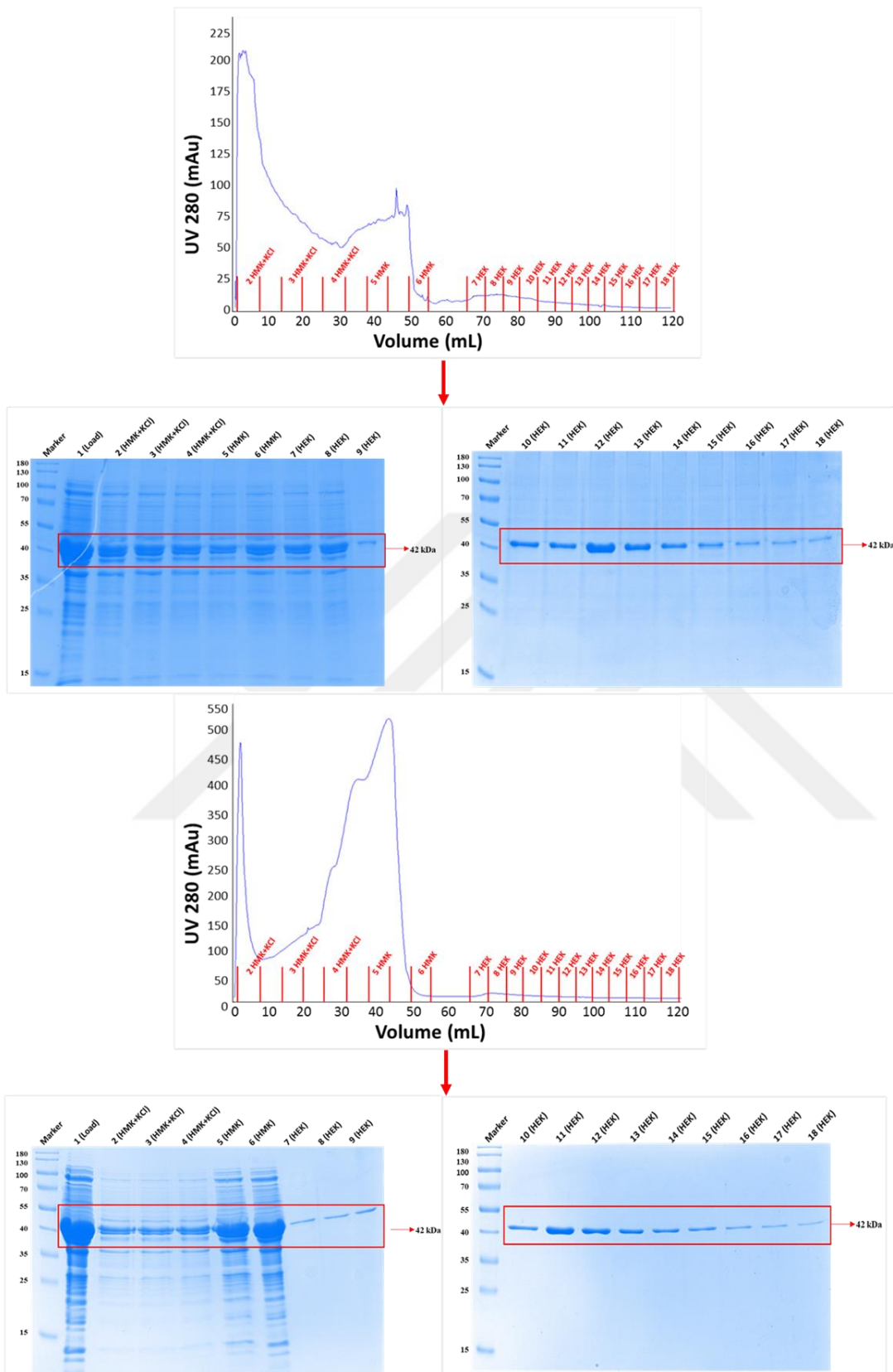


Figure E.3: Replicates of ATP Affinity Purification Chromatograms of DnaK₃₉₂ (above), DnaK₃₉₂ SDS-PAGE results from ATP affinity chromatography (below).

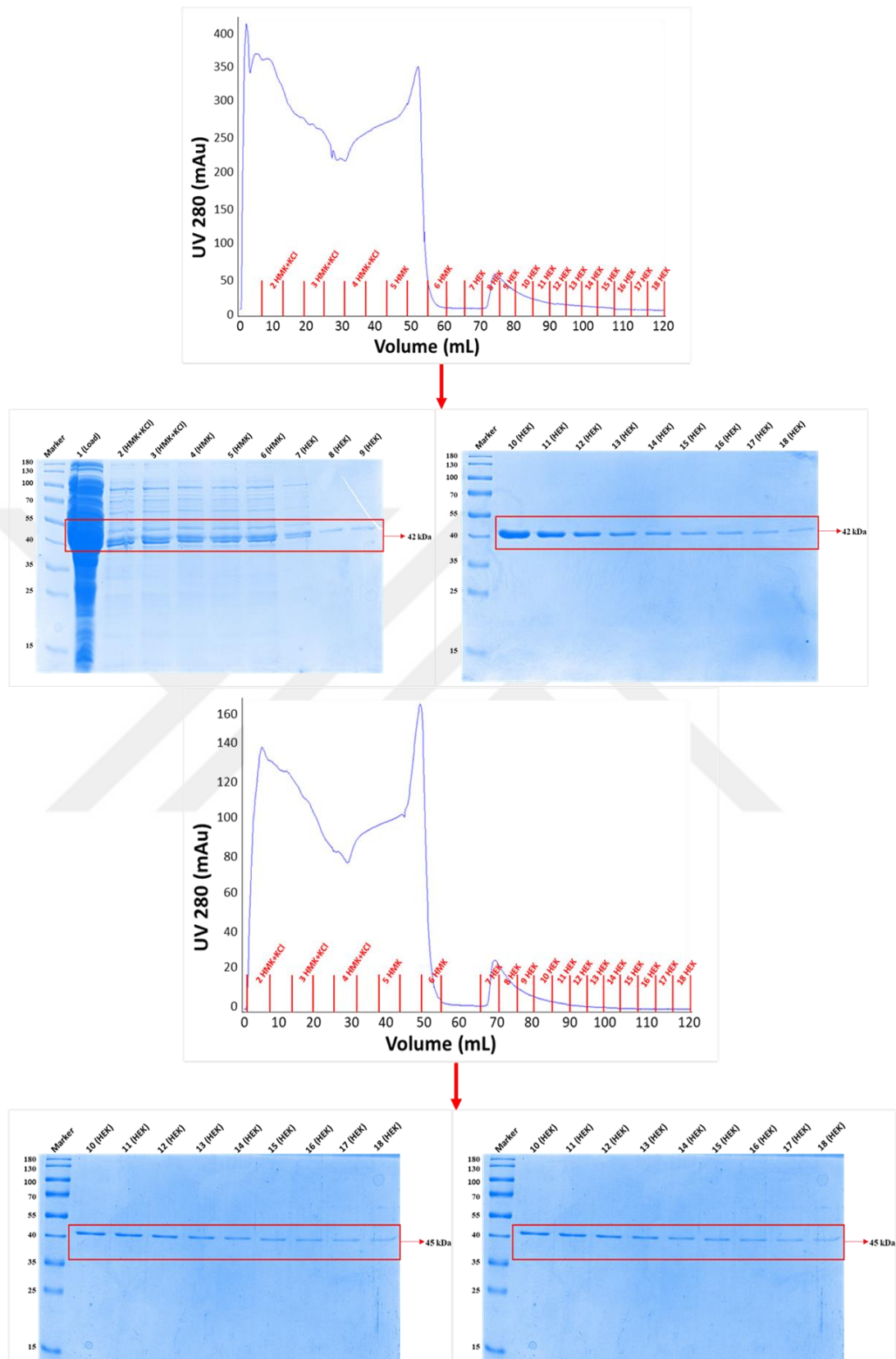


Figure E.4: Replicates of ATP Affinity Purification Chromatograms of DnaK388 (above), DnaK388 SDS-PAGE results from ATP affinity chromatography (below).

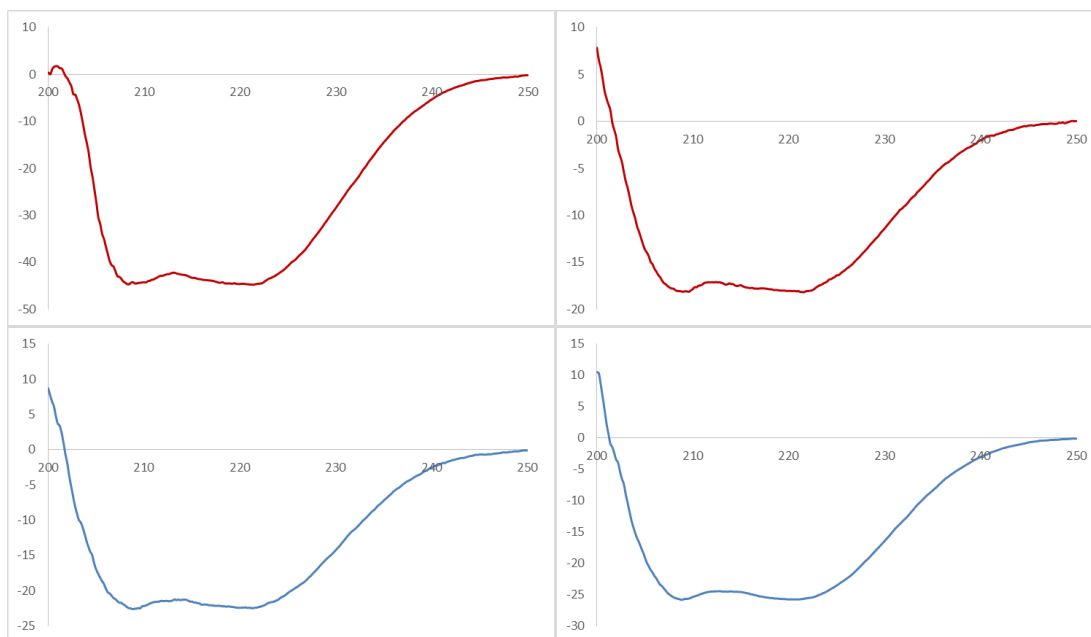


Figure E.5: Replicates of Circular Dichroism spectra results of DnaK₃₉₂ (above) and DnaK₃₈₈ (below).

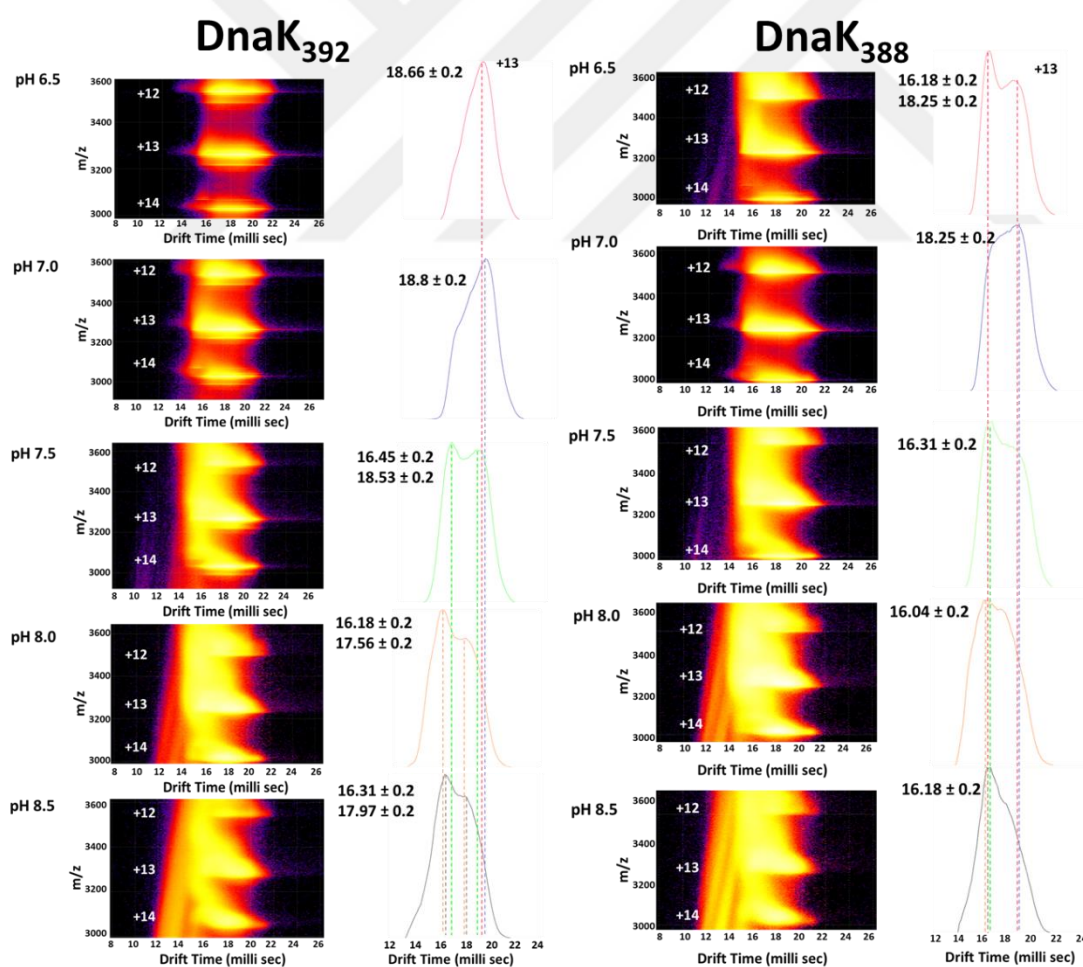


Figure E.6: Replicates of IMS analysis of purified DnaK₃₉₂ (left) and DnaK₃₈₈ (right) protein in a range of pH values. The three-dimensional IMS spectra are on the left, and the drift time distributions are on the right.

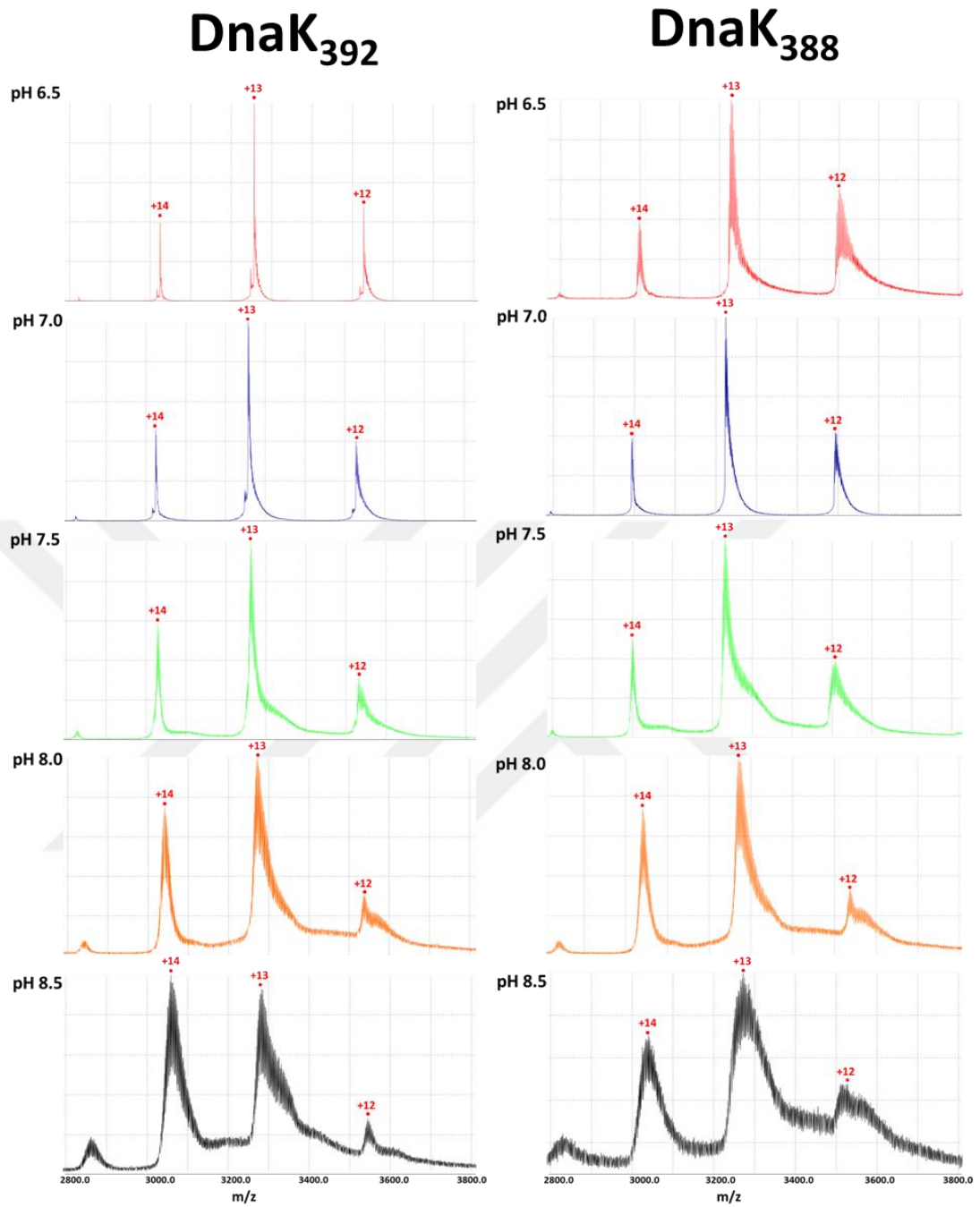


Figure E. 7: Replicates of charge state distributions of purified DnaK₃₉₂ and DnaK₃₈₈ proteins in a range of pH values.

CURRICULUM VITAE



Name Surname : Melis KORKMAZ
Place and Date of Birth : Bakırköy- İSTANBUL / 01.06.1992
E-Mail : meliskorkmaz@hotmail.com.tr

EDUCATION :

- **B.E.** : 2015, Istanbul Bilgi University, Faculty of Engineering and Natural Sciences, Genetics and Bioengineering

PROFESSIONAL EXPERIENCE AND REWARDS:

- 02/2016 – 11/2018 Istanbul Technical University, İstanbul – 1007 KAMAG TUBITAK Project Biosimilar Drug Development, Scholar
- 03/2014 – 07/2014 Florance Nigthingale, İstanbul - Genetics Laboratory and Pathology Laboratory, Intern
- 06/2013 – 08/2013 International Centre for Genetic Engineering and Biotechnology (ICGEB), Cape Town – Cancer Laboratory, Intern
- 06/2013 – 08/2013 Ekici Cheese Factory, Antalya - Intern

LABORATORY SKILLS

Downstream processing of monoclonal antibody production process; homogenization, advanced degree Fast protein liquid chromatography (FPLC-GE Healthcare Äkta Avant_25), secondary structure analysis with Circular Dichroism (CD), beginner of High Performance Liquid Chromatography (HPLC), beginner of Ion Mobility Mass Spectrometry (IM-MS). Isolation of DNA and RNA, SDS-PAGE, Western Blotting, PCR applications, Agarose gel electrophoresis system, Bradford Assay, Nanodrop.

LANGUAGES

English – Advanced Degree

Japanese – Beginner

Germany – Beginner

Turkish Sign Language – Beginner

INTERESTS

Aikido (2.Dan), Drummer, Swimming